August 2021

Water Age, Water Chemistry, and Microbial Populations in a Drinking Water Distribution System

Max Spehlmann
University of Wisconsin-Milwaukee

WATER AGE, WATER CHEMISTRY, AND MICROBIAL POPULATIONS IN A DRINKING WATER DISTRIBUTION SYSTEM

by

Max Spehlmann

A Thesis Submitted in

Partial Fulfillment of the

Requirements for the Degree of

Master of Science

in Freshwater Sciences & Technology

at

The University of Wisconsin-Milwaukee

August 2021

ABSTRACT

WATER AGE, WATER CHEMISTRY, AND MICROBIAL POPULATIONS IN A DRINKING WATER DISTRIBUTION SYSTEM

by

Max Spehlmann

The University of Wisconsin-Milwaukee, 2021
Under the Supervision of Professors James T. Waples, PhD and Ryan J. Newton, PhD

Microbes in tap water play a crucial role in pipe corrosion, human health, and water aesthetics. Because instances of tap water borne illnesses are on the rise in the USA, and many water distribution systems are reaching the end of their design lifespan, research leading to a better understanding of microbial growth and colonization is being actively pursued by many labs (EPA 2002; Miller et al. 2012). In the past decade, several studies have tracked the microbial community change of entire water distribution systems using high throughput sequencing technology (Ma et al. 2020; Perrin et al. 2019). System-scale community microbiology data has shown clear seasonal trends in microbial drinking water taxa. This study utilized similar genomic methods to characterize the planktonic (free-floating) microbial community in the drinking water of the North Shore Water Commission distribution system, just north of Milwaukee, Wisconsin.

As treated water moves through a pipe system, residual microbes from the source water may multiply, or microbes may enter the flowing water from the biofilm covering the pipe wall (Rittman and Snoeyink 1984). American treatment plants seek to deactivate all microbes in the finished water; whereas, European systems focus on removing nutrients from the finished water, especially ammonia, manganese, and dissolved oxygen: As a result, microbes sloughing from the biofilm tend to regrow quicker in American systems, i.e., the water is more unstable, than microbial growth in European systems.

The overall effect of retention time, or water age, on microbial communities is not clearly understood in American or European systems. As disinfectant residuals decline, and exposure to pipe biofilms rises, microbial regrowth and microbial deposition are hypothesized to cause the total microbial load to rise (Wang et al. 2014). Furthermore, certain taxa such as *Sphingomonas*,

Nitrospira, *Mycobacterium*, and *Hyphomicrobium*, have been shown to positively correlate to water age (Chan et al. 2019). However, because water age (retention time) is typically only inferred from spatial data, greater precision in water age measurements will help to characterize microbial community changes with age, and thus improve the understanding of engineering design that impact potential health risks. For example, by identifying regions of a distribution system with chronically high water age, engineers could schedule more frequent hydrant flushing to prevent biofilm formation.

Elucidating water age is a difficult task: Hydrologic models can be used to estimate water age; however, few drinking water systems have models, and those that exist are rarely calibrated with chemical tracers and are based on several untested assumptions (Waples et al. 2015). This study employed a newly designed protocol to measure water age using naturally-occurring radionuclides (Waples et al. 2015). These temporal data combined with 16S rRNA gene sequencing offer insights into microbial growth in a full-scale drinking water system.

Dedicated to

Bruno Jaselskis, PhD.

My Grandpa.

TABLE OF CONTENTS

LIST OF FIGURES

LIST OF TABLES

LIST OF ABBREVIATIONS

AOC – Assimilable Organic Carbon

BCD – Bray Curtis Dissimilarity

CPM - Counts Per Minute

DBP – Disinfection By-Product

DPM – Disintegrations Per Minute

EPA – Environmental Protection Agency

EPS - Exoplymeric Substances

NSWC – North Shore Water Commission

PCR – Polymerase Chain Reaction

qPCR – Quantitative Polymerase Chain Reaction

SLG – Sphaerotilus-Leptothrix microbial Group

UMB – Ultra-MicroBacteria

ACKNOWLEDGEMENTS

First and foremost, I would like to acknowledge Dr.'s James Waples and Ryan Newton for being great advisors. I began this project having little to no experience with radiochemistry or genomics. My advisors provided me with resources to learn the lab techniques necessary for this project. I began my tenure at UWM by taking a trip to Boston to visit the lab of Dr. Ameet Pinto at Northeastern University. There, I worked under the tutelage of his PhD student, Solize Vosloo. With Solize, I learned how to properly sample drinking water to reduce any risk of contamination. Upon my return to UWM, I was guided by many other graduate students and post-docs, namely Lou Lamartina, Dr. Adelaide Roguet, Dr. Shuchen Feng, and Dr. Jill McClary. I was also taught important techniques such as PCR, by our lab manager, Dr. Patricia Bower, and by the visiting professor, Dr. Kazuaki. Throughout the entire program, the Newton lab was kept in good operating condition by the lab managers, Melinda Bootsma and Deb Dila. Before beginning my research, I was awarded funds from both The Water Council, and Sigma Xi to purchase supplies. I was also granted two scholarships through UWM: The Watertech of America Scholarship In Memory of Eugene VandenHeuvel Fund and The Loescher Great Lakes Scholarship. In preparation for field sampling, Randolf Mentzer the machinist at SFS, created some of the pieces needed for the DNA sampling apparatus. During the sampling campaign, Eric Kiefer, the head of the Glendale water treatment plant, helped tremendously by opening hydrants on each sampling date, and by testing for chlorine concentration. Garrett Scapellato, an undergraduate, served as my research assistant and assisted with the microscopy work. Dr. Laodong Guo helped us to filter a water sample to 1 nm using a unique centrifuge. Nathan Van Ee, a fellow master's student helped me to model the genomic data in R. Dr. McNamara allowed

us to use his 16S data collected from the biofilm of Milwaukee pipes, and also served on my thesis committee. The support staff at SFS, especially Nina Ottman, Linda Horbinski, Jenna Jazna, and Mallory Kaul, all provided logistical support for my graduate education. Finally, I would also like to thank my mother and father for providing for me and giving me a strong education.

CHAPTER 1 – INTRODUCTION

Water Distribution in the United States:

Construction of Water Distribution Systems

The first water distribution system in the United States was built in Boston in 1652. It was made from wooden pipes and its intended use was for fire protection. As water distributions expanded to serve growing populations, pipes needed to be made of stronger materials to withstand higher water pressure. Iron became the preferred pipe material beginning in the early 1800s, and in 1804, Philadelphia created the country's largest iron water distribution system. Other municipalities followed suit, and in the 20th century, water pipes were built using a variety of materials such as, asbestos cement, ductile iron, reinforced concrete, galvanized steel, and lead. Today, many municipalities are deciding whether or not to replace their older steel pipes with plastic or iron (Tabuchi 2017). Other materials, such as brass, copper, and stainless steel are also permissible in the United States (NSF International 2001).

Treatment

In the late 19th century, the germ theory of disease was becoming increasingly accepted in the public sphere: And in 1880, researchers identified the causal agent of typhoid to be a microbe in drinking water, *Salmonella typhi.* Many American cities experienced problems with typhoid fever, and as a result there was increasing interest to treat drinking water (Safe Drinking Water Committee and National Research Council 1977). Consequently, in the late 1800s, treatment plants began to incorporate new filtration steps, most notably slow sand filtration, and rapid filtration with chemical coagulation (National Research Council 2002). By the early 20th century, most large American cities had installed some form of treatment technology in their water plants, and these implementations were largely successful in decreasing bacterial colony counts.

In 1908, calcium hypochlorite, conventionally used as a bleaching powder for paper mills and textile factories, was introduced for use in the water plant at the Chicago Stock Yards. The ability of chlorine to cheaply deactivate almost all bacteria made it an enticing choice for cities, and later that year, Jersey City, New Jersey began using chlorine in its treatment plant (National Research Council 2002). Chlorine was rapidly adopted by most American cities, and many years later, in 1989, the EPA mandated that a residual disinfectant concentration in a distribution

system, measured as total chlorine, combined chlorine, or chlorine dioxide must be maintained (EPA 1989). Chlorine is a highly reactive halogen, and can cause cellular damage in humans; as a result, the EPA dictates maximum allowable levels of chlorine residuals in water, which is currently set to 4 mg L^{-1} (EPA 2018). In the United States, all large water treatment systems (serving greater than 10,000 people) use some form of chlorine as a disinfectant, usually sodium hypochlorite, or chloramines (Chlorine Chemistry Council 2003)

As detection technology became increasingly precise, the EPA enacted stricter guidelines for water quality testing. There are currently hundreds of compounds and elements regulated by the EPA, 4 specific organisms (*Cryptosporidium, Cylindrospermosin, Giardia lamblia,* and *Legionella*), and 5 other groups of organisms (heterotrophic plate count, mycobacteria, coliforms, viruses, and cyanobacterial microcystin toxins). The EPA also regulates disinfection byproducts (DBPs) that form after chlorine reacts to organic compounds, which are known to be carcinogenic (EPA 2018). Water treatment plant operators are under scrutiny to ensure that they are providing water that is both chemically and biologically safe. Operators must ensure that they are using enough disinfectant to hinder the growth of undesirable microbes, but not too much, lest they generate too many DBPs.

Planktonic Microbial Growth

With existing technology, modern treatment plants successfully deactivate most microbes post treatment. As finished water travels to the consumer, several processes occur that can encourage the growth of any remaining microbes ("regrowth"), likewise, exposure to pipe walls may cause microbes to enter the finished water. Therefore, water at any point in the distribution system may vary biochemically from finished water.

The final disinfectant step in the treatment plant kills or damages most of the biomass in finished water. Because no treatment plant is 100% effective at removing all nutrients, and, in fact, some treatment plants *add* nutrients to finished water (e.g. orthophosphate, added to prevent lead leaching), water leaving the treatment plant affords open niches to microbes downstream (Nescerecka et al. 2014). As water travels through the pipe network, it is exposed to pipe surfaces, which are usually covered by a biofilm. The interaction of chlorine on biofilms is not clear, but in most cases it seems to inhibit sloughing from the biofilm (Wang et al. 2012). Over time, chlorine reacts with organic carbon to form assimilable organic carbon (AOC), and

consequently, the chlorine residual declines (Nescerecka et al. 2014). The friction of flowing water moving across the biofilm releases sediments (organic carbon, and metal ions) which further contribute to the nutrient pool in the flowing water (Prest et al. 2016). The available nutrient pool, the chlorine residual, and contact time with the pipe biofilm have all been shown to impact the abundance and composition of microbes in the finished water.

Recent research has shown that although changes in the planktonic microbial community are detectable, a core microbial community remains present throughout the system (El-Chakhtoura et al. 2015). In samples from a distribution system that uses biofilters, the core community was composed mostly of taxa originating from the filters (Lautenschlager et al. 2013). In systems that do not use biofilters, most microbes seem to originate from the pipe biofilm (Chan et al. 2019). Distance between sampling stations is clearly important: however, changes in alpha diversity are not significant until sampling points are separated by long distances (> 46 km) (A. Pinto et al. 2014). Several studies have shown that seasonal changes in the core microbiome correlate well with air temperature (A. Pinto et al. 2014; Perrin et al. 2019; Ma et al. 2020). Although the bacterial community remains mostly stable, biomass seems to clearly increase with increasing distance from the treatment plant (Nescerecka et al. 2014)

The conclusions drawn from these studies suggest the following three general characteristics of microbial communities in drinking water treatment system, a stable core microbiome grows in bulk water; rare taxa originate from the biofilm and change stochastically; and, microbial loads increase with distance from the treatment plant.

The North Shore Water Commission

After WWII, the population of Glendale, a northeastern suburb of Milwaukee, began to rise sharply. The Town of Milwaukee, authorized the city of Glendale to exist on its own charter in 1950. After some legal disputes regarding the ownership of water mains, Glendale instated its own water utility in 1959 (Public Service Institute of Wisconsin 1968). The North Shore Water Commission (NSWC) was created to provide water for Glendale, Fox Point, and Whitefish Bay, each of which operate their own water utilities. The commission built a water filtration plant, as well as a raw water pumping station, which pumps Lake Michigan water. In 2018, the NSWC pumped a total of $1.23 * 10^9$ gallons, by way of comparison Milwaukee Water Works, pumped $7.53 * 10^9$ gallons (North Shore Water Commission 2018; Milwaukee Water Works 2018).

The NSWC pulls water from an intake crib in Lake Michigan. The crib is covered with bar screens and contains a mussel control system to prevent zebra and quagga mussels from colonizing the pipes. After travelling several miles west, the water enters the main treatment facility in Glendale. The first step in the treatment process is the addition of aluminum sulfate and a polymer to promote the settling of solids. The water then meanders through a series of rectangular basins where solids settle out. The water then passes through rapid sand filters to remove any remaining particulate matter. Afterwards, fluoride is added to the filtered water, then intermediate pumps force the filtered water through an ultraviolet disinfectant system to inactivate pathogens. Sodium hypochlorite is added to the water as a secondary disinfectant, and the water then sits in chlorine contact-time clear-wells.

After allowing the chlorine time to inactivate microbes, high service pumps pull the disinfected water into a chemical feed vault where ammonium hydroxide and phosphate are added. Ammonium hydroxide converts free chlorine from the sodium hypochlorite into chloramines. Phosphate is added to prevent lead and copper fixtures from corroding into the finished water. At this point the water is finished, and passes through the main facility to enter the distribution systems of either Fox Point, Glendale, or Whitefish Bay (North Shore Water Commission 2020).

Drinking Water Microbiology:

To make sense of patterns in the microbial community observed in this study, a basic understanding of the dominant groups of microbes observed is necessary. In microbial taxonomy, the phylum is the broadest group of classification within the domain of bacteria. Bacterial phyla delineate a group of bacteria that "cannot be aggregated to any taxon except Bacteria. (Jumas-Bilak, Roudière, and Marchandin 2009)" From most broad to least, the other taxonomic groups used to describe bacteria are, class, order, family, genus, species. From class to family, the criteria for inclusion are generally defined by historical context. A genus may be functionally defined or based on 16S rRNA gene sequence similarity.

In contrast to the higher organisms, the species concept is less definitive when applied to microbes, mainly because microbes often reproduce asexually. Using morphological differences is also not ideal, because microbes are anatomically simple. The current, most accepted, microbial species definition is the following, "a distinct group of strains that have certain

distinguishing features and that generally bear a close resemblance to one another in the more essential features of organization." Furthermore, a "strain" is composed of the descendants of a single isolation in pure culture (Garrity 2007).

Microbes found in the flowing water of the NSWC system originate from either the source water (Lake Michigan), the pipe wall, or the biofilters from the plant. Because many of the taxa inhabiting the biofilters also colonize the pipe wall, this study focused on those microbes associated with the lake and pipe-wall. Further information regarding these taxa are described below.

Lake Microbes

The most common lake phyla are *Proteobacteria, Actinobacteria, Bacteriodeta, Nitrospirota, Cyanobacteria, Planctomycetota, Verrumicrobia, Deinococcota,* and *Bdellovibrionota* (Newton et al. 2011). The *Proteobacteria* are ubiquitous environmental organisms and are very common in freshwater ecosystems. *Actinobacteria* may compose >50% of all microbes in surface waters, many are in the ultra-micro-bacteria size range (<0.22 μm diameter) and some may be symbionts of other bacteria. *Actinobacteria* are also resistant to UV desiccation and are spore formers (Newton et al. 2011). The *Bacteroidota* are the third most common lake phyla: they compose 10 – 30% of lake microbes, commonly are the primary degraders of complex carbohydrates, and can exist symbiotically with higher organisms.

Several groups of nitrifying microbes, namely, the phylum, *Nitrospirota,* and the genera, *Nitrobacter* and *Nitrospira* are commonly found in the sediment of Lake Michigan. These groups include ammonia oxidizers, nitrite-oxidizers, and anaerobic ammonia oxidizers (anammox), which combine nitrite and ammonia to form dinitrogen gas. The addition of the nitrogenous chloramine molecule as a primary disinfectant allows several groups of nitrifiers to grow in finished water. Free ammonium, from the chloramine molecule, is readily oxidized by the slow-growing ammonia-oxidizing bacteria or archaea. After ammonia is oxidized to nitrite, nitrite is in turn oxidized to nitrate by organisms of the genera *Nitrobacter* and *Nitrospira.* Organisms within *Nitrobacter* all have similar physiologies and are ellipsoidal to rod-shaped and are common in soil and marine systems (Koops et al. 1991). After nitrogen has been oxidized to nitrate, a group of denitrifying organisms, such as those in the genus *Pseudomonas,* can reduce nitrate to either NO gas, or dinitrogen, both of which may degrade the pipe wall.

The *Cyanobacteria* are photoautotrophs that use chlorophyll a and b to reduce H_2O: despite their dependence on light, small numbers of *cyanobacteria* are often found in drinking water systems (Potgieter et al. 2018; Prest et al. 2016). In the absence of light, these organisms may grow very slowly by switching to a chemotrophic growth phase facilitated by the oxic conditions of flowing water (Brenner et al. 2005); some cyanobacteria produce resting spores in conditions of light limitation (Wilmotte and Herdman 2001). .

Finally, the three least common lake phyla are the V*erromicrobia* and the *Deinococcus*, and the B*dellovibrionota*. The *Verrumicrobia* represent, on average 1 – 6% of the species recovered from freshwater lakes. They are found in acidic environments and are copiotrophs (found in high nutrient conditions): Like *Planctomycetes*, they have rudimentary intracellular compartments, and may use methane as a carbon source. *Deinococcus* is a little-understood phylum of chemoorganotrophic microbes with unusually thick cell walls (50 – 60 nm). They are found in diverse environments, and are difficult to cultivate (Murray 2004). *Bdellovibrionota* are likewise little studied. They are known to be obligate predators of gram-negative bacteria and are commonly found in aquatic environments (Q.-M. Li et al. 2021).

Pipe Wall

Phyla associated with the pipe wall are shared with the lake group, except for the *Firmicutes, Campilobacterota, Acidobacteria,* and *Patescibacteria* (Kimbell et al. 2021) . The *Firmicutes* are a diverse group of spore-forming microbes. The *Acidobacteria* are abundant in soil ecosystems, are slow-growers, and express many kinds of intracellular transporters which may be advantageous in oligotrophic environments (Kielak et al. 2016). The *Patescibacteria* are a superphylum common in groundwater, they are often small enough to be considered UMB and have reduced genomes (Tian et al. 2020).

Pathogens

Certain pathogens are well-adapted to the low-nutrient concentrations in finished drinking water: They may persist in biofilms for long periods of time, and either release cyclically in response to temperature change, or slough at a constant rate. Primary pathogens are those that may infect healthy individuals; whereas, opportunistic pathogens are ones that infect immunocompromised individuals (EPA 2002). Primary pathogens include *Salmonella typhi* which cause typhoid fever,

Vibrio cholerae, which cause cholera, and *Legionella pneumophila,* which cause Legionnaire's Disease. Legionnaire's disease is becoming increasingly common in the United States, and *Legionella* was therefore analyzed using quantitative PCR (qPCR) in this research to determine its exact concentrations in the drinking water (Weekes and Weekes 2017). Opportunistic pathogens include members of the *Mycobacterium avium* complex, and *Pseudomonas aeruginosa,* both of which may cause pneumonia, and various *Flavobacterium spp.,* which may cause meningitis.

Studying the NSWC System:

The NSWC has not yet performed full-scale genetic analyses of their finished water. Heterotrophic plate counting monitoring, required by law, is useful for detecting the presence of bacteria that rely on organic nutrients for growth; however its utility in describing microbial community composition and abundance is severely limited (Allen, Edberg, and Reasoner 2004). 16S rRNA gene analyses provides a first-time glimpse into the microbial ecology of this system. Coupling these microbial data with water chemistry and water age data allowed for the derivation of meaningful quantitative measurements of microbial cell concentration, microbial community change, and disinfectant decay.

Chapter Outline

During the summer and fall of 2020, 4 sites in the Whitefish Bay section of the NSWC were sampled on a bi-weekly basis (fig. 1). At each station, both community microbiology, and radiochemistry measurements were taken. In chapter two, the results of the 16S rRNA gene sequencing are discussed and the microbial community in the system is characterized. In chapter three, the radiochemistry data is explored. Finally, in chapter four, data from these two lines of inquiry are combined to explore the ways in which the microbial community changed both throughout the samplings season, and in relation to water age and water chemistry.

CHAPTER 2 – CHARACTERIZING THE MICROBIOLOGICAL COMMUNITY

Introduction, Gene Analyses:

To characterize the microbiome in this study, a universal marker gene analysis was selected. Universal marker genes are shared across most known microbial phyla: the sequences contain a variable region, which delineates among microorganisms, flanked by conserved regions, which allow for the isolation and amplification of the variable region in mixed microbial communities. In a polymerase chain reaction (PCR)-based marker gene study, two primers are used: one primer is the DNA complement to the upstream conserved sequence region, and the other primer is the complement to the downstream conserved region. Because conserved regions are not identical across all microbes, the primers used can introduce bias (Knight et al. 2018), but generally this method has been shown to provide a reasonably accurate representation of the microbial composition in most environments.

The 16S rRNA gene was selected as the marker gene in this study. This marker gene codes for an RNA molecule of the archaeal and bacterial ribosome with a molecular weight of 16 Svedbergs. Most bacterial and archaea contain a linearly arranged 16S rRNA gene, with conserved sequence regions; therefore, it is used as a common marker gene in microbiome studies (Knight et al. 2018). In recent years, 16S rRNA gene analysis has become increasingly prevalent as a method to describe prokaryotic taxonomy. The method is faster, simpler, and less tedious than culture-based methods and consequently, it is one of the most widely used classification techniques in prokaryotic identification and systematics (Brenner et al. 2005). Because many labs target the 16S rRNA gene in drinking water studies, effective primers, and DNA isolation protocols, have been developed. Primers designed to amplify the V4 region within the 16S rRNA gene were chosen in this study because they capture both archaeal and bacterial microbes (Parada, Needham, and Fuhrman 2016; Walters et al. 2015).

After collecting, and isolating DNA, PCR was used to amplify the region between the two primers. After amplification, the marker genes were sequenced. The illumina platform, which is fast, cost-effective, and accurate was selected to sequence the DNA in this study. The

sequence data was then processed and analyzed to yield high-resolution community abundance data.

Introduction, Sampling Strategy:

Four hydrants within the Whitefish Bay distribution were chosen to sample throughout the study period. Each hydrant was situated above an iron water main and were separated by roughly 1.2 km (table 1). The distance between stations was determined by following the shortest possible length of water main between stations. The first station (Station 1) was about 1 km from the Glendale treatment plant, and the fourth station (Station 5) was about 6 km distal (fig. 1). The fourth station was situated at a dead-end node, and, consequently was likely to contain old water.

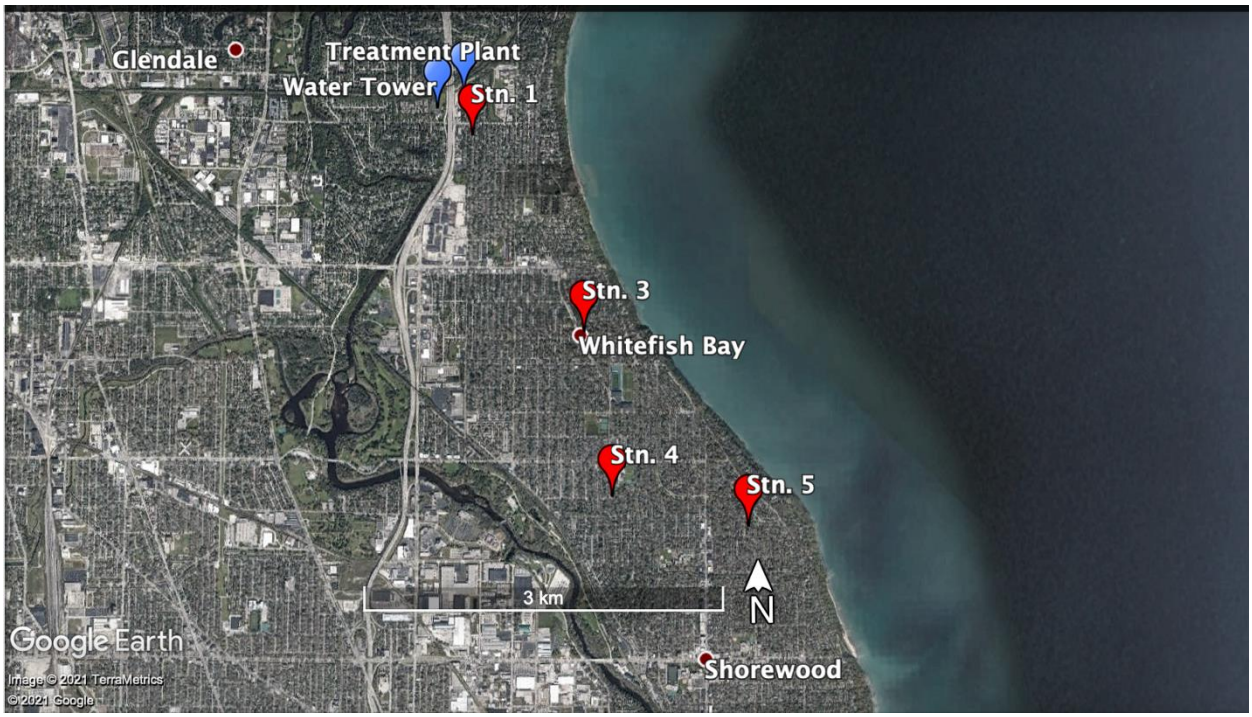

Figure 1: Map of sampling locations and treatment plant in Whitefish Bay, Wisconsin. NB, "station 2" was not included in this study.

The hydrants were sampled from August through December of 2020, and each station was sampled approximately 7 times throughout the study (Table 1). For a complete list of the dates on which samples were collected, see table A1.

Table 1: Station location and number of times sampled for genetic data.

Station name	Address (in Whitefish Bay, WI)	Number of microbial samples
Treatment Plant	400 W Bender Rd (Glendale, WI)	3
1	6142 N Lydell Ave	7
3	902 E Lexington Avenue	8
4	1100 E Courtland Pl	7
5	4524 N Frederick Ave	7

In addition to collecting water for 16S sequencing, the planktonic cell concentration was measured using a fluorescent dye stain, DAPI, which stains DNA. To describe the water quality in the system, basic chemical parameters were also measured at each station. And finally, one pathogen of interest, *Legionella*, was quantified using a qPCR assay. After obtaining all the results, the following analyses were performed. Replicate 16S samples were compared to determine the precision of the microbial community data. Then, to determine the extent to which microbial diversity varied by pipe distance, the community diversity across sampling locations was analyzed. The planktonic community composition in the system was explored and compared to similar studies, and a core community was identified. The community data was then compared to the water age and chemistry data to determine the extent to these parameters shaped the microbial community (chapter 4).

Methods, Microbiological and Water Chemistry Sample Collection:

Samples were collected between the hours of 8 and 10 am in the Glendale section of the NSWC system. Four sites were chosen, and three sites were sampled weekly for 12 weeks. At each field station, a fire hydrant was opened and allowed to discharge for approximately five minutes, or until the water appeared clear. Then, the pressure was lowered, and water for microbial samples was collected in two 20L carboys. Spot samples were taken with an EXO Sonde for basic water quality parameters. Chlorine was measured using a Hach test for free and total chlorine (Mott 2016). In the lab, the water was filtered through enclosed 0.22 µm Sterivex (Millipore, polyethersulfone) filter cartridges attached to peristaltic pumps, which drew water from the

carboy through the filter. Approximately 3L of water was passed through each filter. After allowing the filter to dry, the filter was kept at -20°C until extraction.

Methods, DNA Extraction:

Samples were extracted using a modified Qiagen porewater extraction kit procedure (Ushio 2018). After filtration, the outlet of the Sterivex filter was capped using capillary tube wax, and zirconia beads were aseptically inserted into the cartridge. Next a lysis buffer consisting of 220 µl of PBS, 200 µl of Buffer AL (Qiagen), 400 µl of Power Water 1 (Qiagen), and 20 µl of 20 mg/ml Proteinase K was prepared. 840 µl of the lysis buffer was pipetted into each filter cartridge. The filters were briefly vortexed on high, and then incubated at 50 rpm at a temperature of 56°C for thirty minutes. The cartridges were then vortexed on high for three minutes. Then, immediately following vortexing, microcentrifuge tubes were placed into a 50 ml collection tube. The filter cartridge was placed into the 50 ml collection tube with the uncapped influent port facing downwards, into the 650 µl microcentrifuge tube. Then, working quickly, the 50 ml collection tube was capped and spun in a centrifuge at 4°C at 1400G for 3 minutes. The cartridge filter was then discarded and the 650 µl microcentrifuge tube containing the effluent was further purified using the Qiagen DNEasy Power Water kit and the associated protocol. Two slight modifications were made to the protocol: at the silica column binding step, effluent from two filter cartridges were combined in the silica spin column. In the final elution step, 30 µl of elution buffer was added on to the silica membrane, allowed to incubate for five minutes, and then centrifuged. The process was then repeated, so that each sample was suspended in 60 µl of elution buffer.

To amplify the V4 region of the 16S rRNA gene, the primers 515Fb and 806Rb, and the GoTaq (Promega) polymerase system were used in all PCRs. In the final reaction setup for all samples, a 25 µl reaction volume with 5 µl of template DNA was used. Each sample was run in triplicate. The cycling conditions were as follows: 95°C for 5 minutes, thirty cycles of, 94°C for 45 seconds, 50°C for 1 minute, 72°C for 45 seconds, and finally, 72°C for five minutes (Goodrich et al. 2014). To ensure that the reaction occurred properly, gel electrophoresis was used to verify amplification specificity with a DNA product of around 250 base pairs long. After PCR amplification, the triplicate reactions for each sample were pooled and then cleaned using the AMPure XP magnetic bead kit (Agencourt). The DNA concentration of each combined,

cleaned sample was quantified using a Qubit fluorometer set to high sensitivity. Finally, the pooled and cleaned 16S rRNA gene amplicons were indexed with illumina-specific sequencing primers and sample barcodes. Sequencing was conducted on an illumina MiSeq at the Great Lakes Genomic Center.

In addition to the processing of individual samples, three samples were filtered in triplicate, 10 samples were amplified with PCR in duplicate, and 3 samples of nuclease-free sterile water were processed and sequenced to assess contamination. A filter-pore-size replicate, filtered at 1 nm using a spiral wound S10N1 ultrafiltration cartridge (Amicon/Millipore) was also sequenced.

Methods, Raw Sequence Processing:

The FASTQ files from the illumina sequencer were processed in R using the package, dada2 (Callahan et al. 2016). The primers were removed from all sequences, and the sequences were trimmed to 230 base pairs to remove lower-quality sequence data at the end of the reads. One sample was removed because of a low read quality score. Then, the forward and reverse reads were merged, and any merged sequence with more than 265 base pairs or less than 240 base pairs was removed. Then, the function *removeBimeraDenovo* was used to remove sequence chimeras.

After cleaning and merging the read data, each amplicon sequence variant (ASV) was compared to the Silva database (*release #138*) of microbial DNA to identify the organism from which that ASV was derived. The assignment made to the ASV is known as an operational taxonomic unit (OTU). The combined OTU identification data (which organisms were present) and the count of each OTU (the abundance of each organism in each sample) represents the community composition of the sample. Because the amplification process is inherently stochastic, i.e., each strand of DNA was not amplified uniformly, the abundance of each unique sequence (i.e. organism) present in the sample was normalized to the total number of reads in each sample.

The R package *Decontam* was also used to filter OTUs that were likely to be a result of contamination during sample preparation, and to remove sequences found in the negative controls (Davis et al. 2017). All OTUs with a total count of less than 5 were removed.

Furthermore, because only those OTUs present in multiple samples can be compared across samples, OTUs with a prevalence of 1 were removed as well. After fully processing the sequence data, the total number of unique OTUs diminished by 90% (5,576 OTUs). This level of reduction is not uncommon, other tap-water microbial community studies have processed out 89% of their OTUs for similar reasons (Potgieter et al. 2018).

Methods, DAPI-Stained Cell Counting:

To estimate the total cell abundances, a DAPI dye staining protocol was employed (Noble and Fuhrman 1998). DAPI intercalates DNA and fluoresces under UV light. One ml of tap water was incubated with 15 µl of a DAPI stain for five minutes. The solution was then mixed with 5 ml of PBS and filtered through a 0.22 µm filter (Whatman, Nucleopore). The filter was then mounted on a slide and then photographed under UV light using a Zeiss microscope. 10 photos were taken at random locations on the filter. The photos were analyzed in ImageJ: first the file was converted to 8-bit, then the threshold was adjusted until only cells were highlighted in the software, finally the cells were counted using the *analyze particles* function.

Methods, Legionella qPCR:

A TaqMan qPCR assay developed by Lu et al (2015) was selected to measure the abundance of *Legionella* organisms in the purified DNA (Lu et al. 2015). 20 µl reaction mixtures composed of 10 µl 2x TaqMan Environmental Master Mix 2.0 (Applied Biosystems), 0.25 µM probe, 0.625 µM primers, and 5 µl DNA template were created. The samples were loaded into StepOne Plus qPCR machine (Life Technologies) and the cycling conditions were as follows: 10 min at 95°C, followed by 40 cycles of 95°C for 15 s, 63°C for 110 s. The Ct values were compared to a standard curve to derive the starting concentration of *Legionella* in each sample. The standard curve of this assay yielded a slope of -3.532, a y-intercept of 40.749 cycles, an R^2 of 0.997, and an efficiency of 91.92%. The limit of detection (LOD) was, 5 copies per L, and the limit of quantification (LOQ) was 60 copies/L.

Results & Discussion:

General Water Quality Parameters

The sonde-derived water quality measurements were analyzed to gain a better understanding of the way in which important parameters such as dissolved oxygen (DO) tended to change throughout the study period. The contextual water chemistry data tended to remain within narrow bounds through the course of the study. Free chlorine did not lower markedly until station 5. Specific conductivity generally stayed within a narrow range of values, from 300 – 315 μs/m^2, which is similar to lake Michigan water. The water tended to warm and become less saturated with DO as it moved distally from the treatment plant (fig. 2).

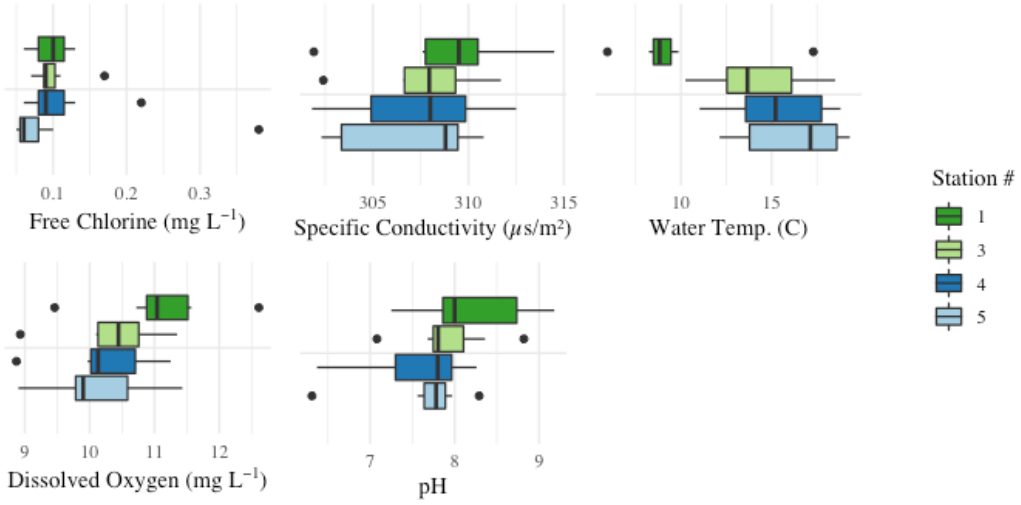

Figure 2: Boxplots of sonde-measured water quality parameters.

At the treatment plant, chlorine is added to finished water at a concentration of 3.2 mg L^{-1}. Before exiting the plant, the chlorinated water incubates in clear-wells to allow the chlorine to deactivate pathogens. Finished water usually enters the distribution system from the clear-wells at a concentration of 0.05 mg L^{-1} free chlorine; however, the exact residual concentration may vary depending on water temperature and pH. At an unknown time around 9/30/2020, an issue occurred in the plant causing excess chlorine to enter the finished water. This variation was measured on 10/01/20, and was especially evident at the most distal station, with a chlorine residual of 0.39 mg L^{-1} (fig. 3).

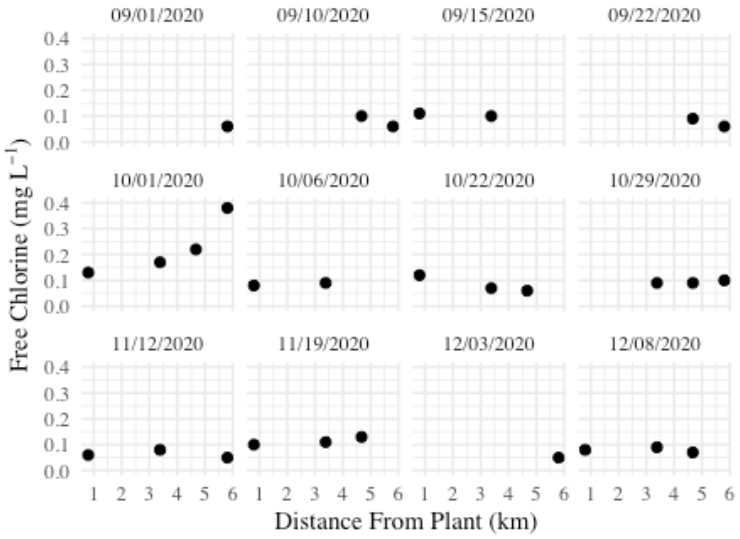

Figure 3: Scatter plots of Free Chlorine (mg L^{-1}) by date.

Water temperature displayed the strongest collection to distance from treatment plant, on average, the water temperature rose 1.2 °C per km (fig. 4).

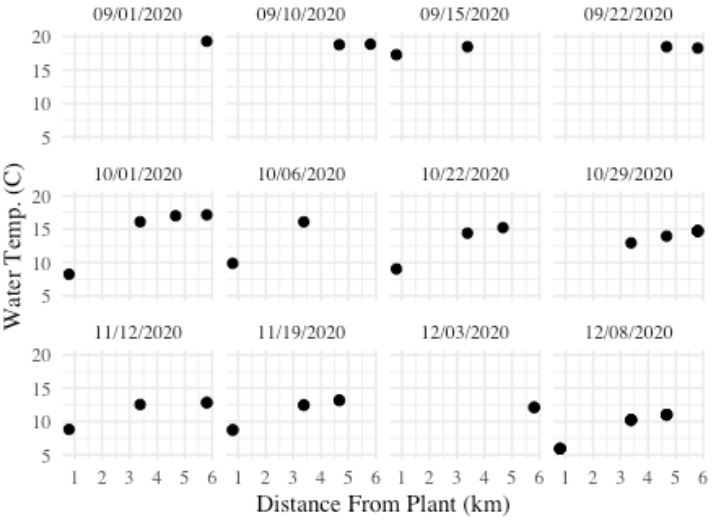

Figure 4: Scatter plots of water temperature (C) by date. The average change in C per km was, 1.2 C/km.

Within sampling dates, dissolved oxygen tended to remain within a narrow range (± 2 mg L^{-1}) (fig. 5).

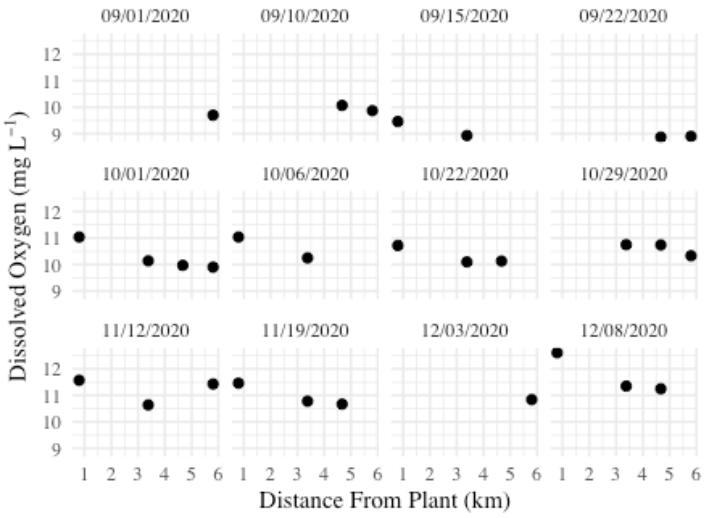

Figure 5: Scatter plots of dissolved oxygen (mg L^{-1}) by date.

The pH tended to remain close to 8. As water heated up in the pipe network, the pH tended to drop slightly (fig. 6).

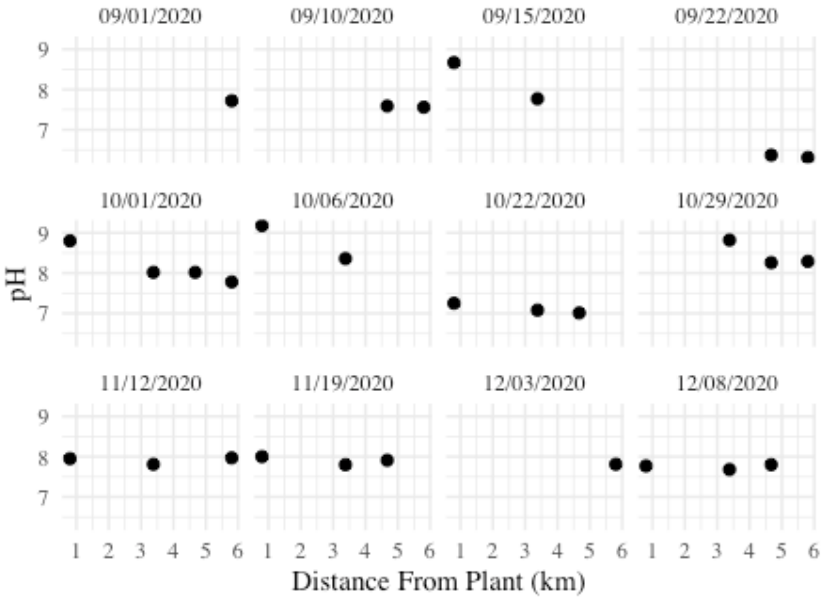

Figure 6: Scatter plots of pH by collection date

Overall, the DO, water temperature, chlorine residual, and the specific conductivity remained stable throughout the study period. The Milwaukee Water Works routinely tests for a suite of 70 chemical parameters, and over a study period of more than 20 years, has not observed significant

fluctuations in any parameter except chlorine, because of road salt intrusion into Lake Michigan (Beversdorf, *personal comm.*).

Cell Concentration:

Because 16S sequencing does not provide absolute measurements of biomass, a DAPI stain was used to determine cell concentrations at each station. The microscopy-measured cell concentrations in distal stations fell within typical ranges measured in drinking water, from 4.61E2 – 1.76E5 cells/ml. Although, the cell concentrations in distal stations were, on average, 7.5 times greater than the cell concentration in the treatment plant, the difference was not significant, most likely because of low sample numbers (fig. 7).

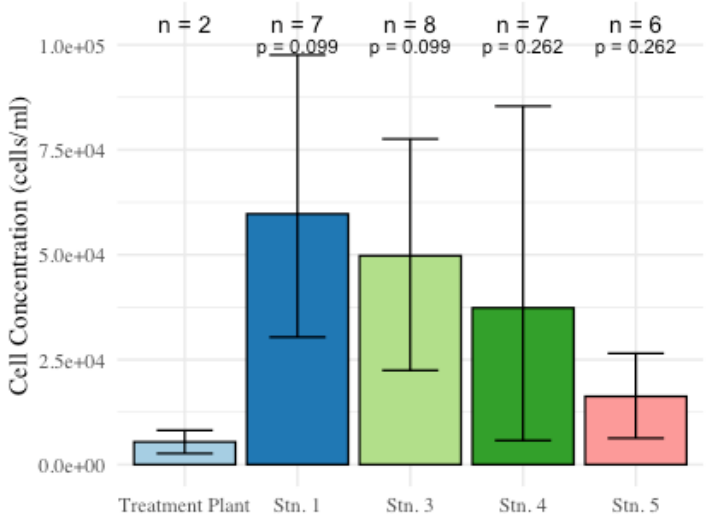

Figure 7: Mean cell concentrations measured at treatment plant and four stations. Error bars are the upper and lower Gaussian confidence limits based on the t-distribution. P-values from independent two-sample t-tests, adjusted using the Benjamini-Hochberg procedure, are displayed above the sample type in reference to the treatment plant.

An independent, two-sample T-Test was used to compare each of the distal stations to the treatment plant: the null hypothesis, that the mean cell concentration between a distal station and the treatment plant could not be rejected. In a system-wide study conducted in Riga, Latvia, Nescerecka et al. (2014) found that the planktonic cell concentration only rose significantly after water had travelled ~15 km from the treatment plant. All the stations examined in this study were within 7 km of the plant; consequently, the cell concentrations observed may be influenced by stochastic processes, such as biofilm sloughing, more so than stable, regrowth processes.

Similarly, Pinto et al. (2014) found that in the Ann Arbor drinking water utility, stochastic processes seemed to dominate microbial communities until stations were separated by 46 km.

16S, Replicate Analysis:

All Samples:

The first analysis performed on the 16S data was to determine the similarity of replicate samples. If the 16S sequencing methodology was 100% precise, then the replicate samples would yield the exact same community abundance data. Disparity between the results of the replicate samples indicates the influence of systematic error on the sequencing results. The Bray Curtis Dissimilarity (BCD), a metric that quantifies the difference in species composition between two sites was used to quantify the dissimilarity between replicate samples. The BCD was computed between all samples of replicate groups, and between all non-replicate ("unique") samples. Between-sample dissimilarity was not significantly different than between-replicate dissimilarity; therefore, the null hypothesis, that the replicate samples are as dissimilar as different samples, could not be rejected (fig. 8).

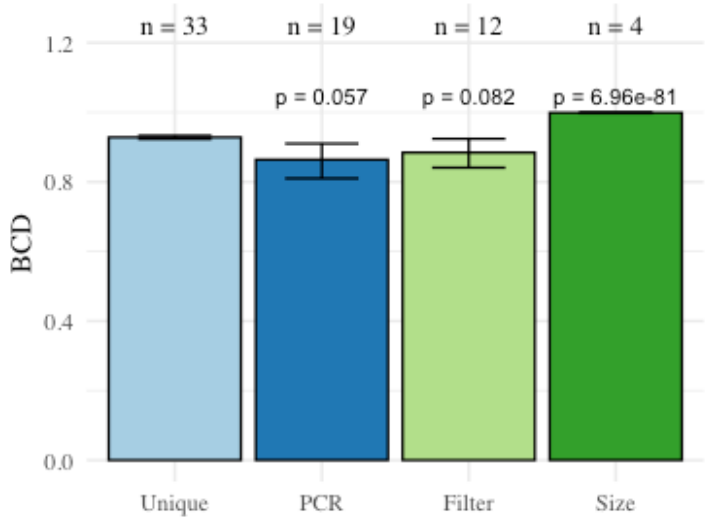

Figure 8: Mean Bray-Curtis Dissimilarity across sample types. Error bars are the upper and lower Gaussian confidence limits based on the t-distribution. P-values from independent two-sample t-tests, adjusted using the Benjamini-Hochberg procedure, are displayed above the sample type in reference to unique samples.

The BCD data suggests that the sequence data may be influenced by low DNA concentrations. Low DNA concentrations increase the likelihood of ASV drop-in and drop-out during PCR. ASV drop-in occurs when an ASV is amplified in one replicate, but not another. ASV drop-out is

the converse: an ASV is not amplified during one of the first rounds of PCR, and so drops out of the analysis pool. For the remainder of the analysis, a consensus sample was calculated from replicate samples by taking the mean abundance from each replicate, except for the pore-size replicate (Butler and Hill 2010).

Pore Size Replicate:

All the samples were filtered using a pore size of 0.22 µm, except for the pore-size replicate, which was filtered at 1 nm using a spiral wound S10N1 ultrafiltration cartridge (Amicon/Millipore). To compare the 1 nm filtered sample to the 0.22 µm sample, the BCD between the size replicates was compared to the BCD between all the unique samples.

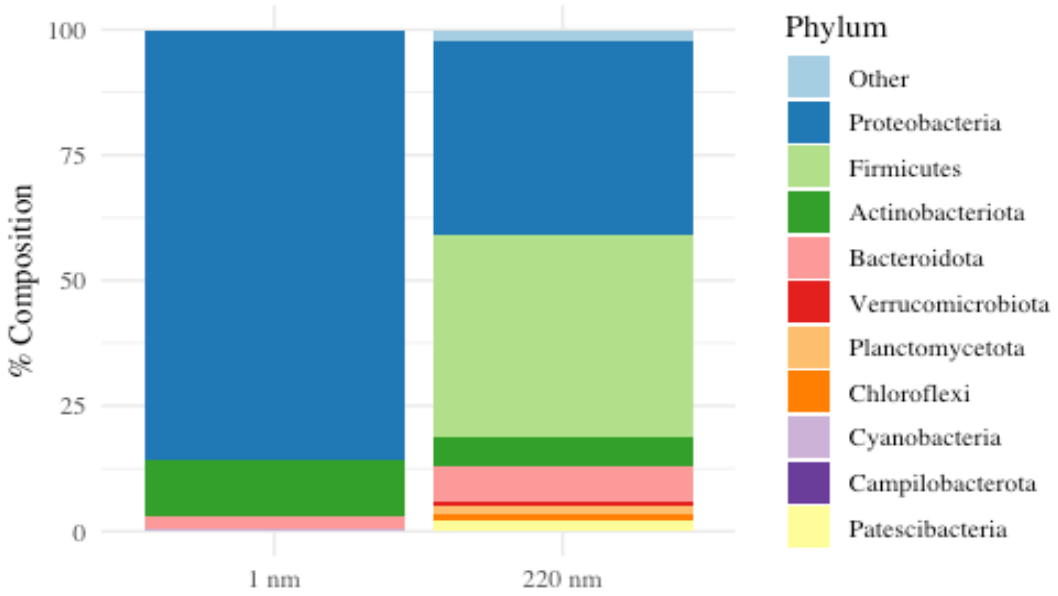

Figure 9: Bar charts of the relative abundance of the top ten phyla between the two filter types. The mean BCD between all unique samples is, 0.93, and the distance between the two filter types is, 0.97. A BCD of 1 indicates that the samples are as dissimilar as possible.

The average BCD between all unique samples was 0.93, and the BCD between the size replicates was 0.97, which suggests that the communities between 1 nm and 0.22 µm are significantly different from the communities 0.22 µm and higher. The community present in the filter blank was also significantly different from both the 1 nm sample, and the 0.22 µm sample. The filter blank contained mostly *Firmicutes* (40%) and *Proteobacteria* (30%). Of the orders present in the 1 nm sample, and not the 0.22 µm sample, the most abundant were *Nitrosococcales, Rhodobacterales, Pseudomonadales, Micropepsales, Microtrichales, Obscuribacterales,*

Frankiales. Members of these orders are often designated ultramicrobacteria (UMB), which are a diverse group of microbes that are typically not captured on 0.22 µm filters. Evidence is being increasingly found which suggest that UMB play a prominent role in oligotrophic environments, consequently, they are likely important in the drinking water microbiome (Lautenschlager et al. 2014; Newton et al. 2011). Furthermore, many microbes are not completely planktonic, a growing body of research is providing evidence that most microbes are found adhering to particles of varying sizes (Characklis et al. 2005). To gain a better understanding of the extent to which microbes vary by particle size, and cell diameter, future studies should perform filtration at several pore sizes.

16S Diversity Analysis:

After computing the consensus microbial community data, the diversity between sites was explored. The diversity of the microbial community was hypothesized to correlate to the distance from the plant. The Shannon diversity index was used to measure diversity because it is more sensitive to rare species than other common diversity indices, such as the Simpson index. The Shannon diversity did not change significantly from station to station, as determined by a one-way ANOVA ($F(3,25) = 0.83$, $p = 0.49$) (fig. 10).

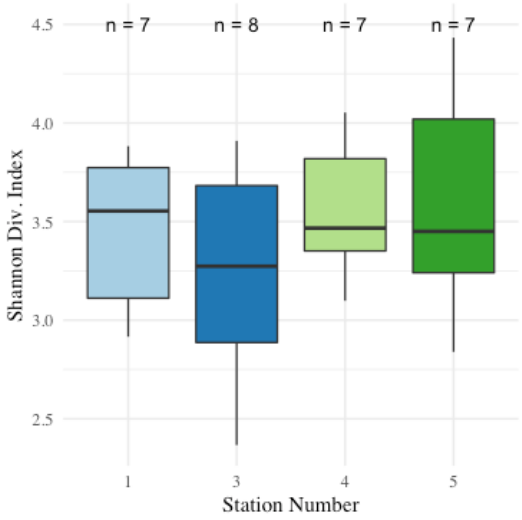

*Figure 10: Boxplots of the Shannon Diversity by station. There were no significant differences between group-means as determined by a one-way ANOVA (*F*(3,25) = 0.83*, p *= 0.49).*

Ranging from 2.4 - 4.43, the Shannon diversity in this study was lower than that of many other systems, which may be reflective of the oligotrophic Lake Michigan source water. In a 2019

study in Sweden, Chan et al., found that the microbial diversity of planktonic microbes in drinking water ranged between 4.5 – 5.25 (Chan et al. 2019). Furthermore, they did not observe significant changes in diversity across stations – but rather, the increase of certain taxa as they moved distally from the treatment plant, such as *Sphingomonas*, *Nitrospira*, *Mycobacterium*, and *Hyphomicrobium.* The same four genera were also detected in this study; however, their relative abundances only increased with distance on six of the transects (fig. 11).

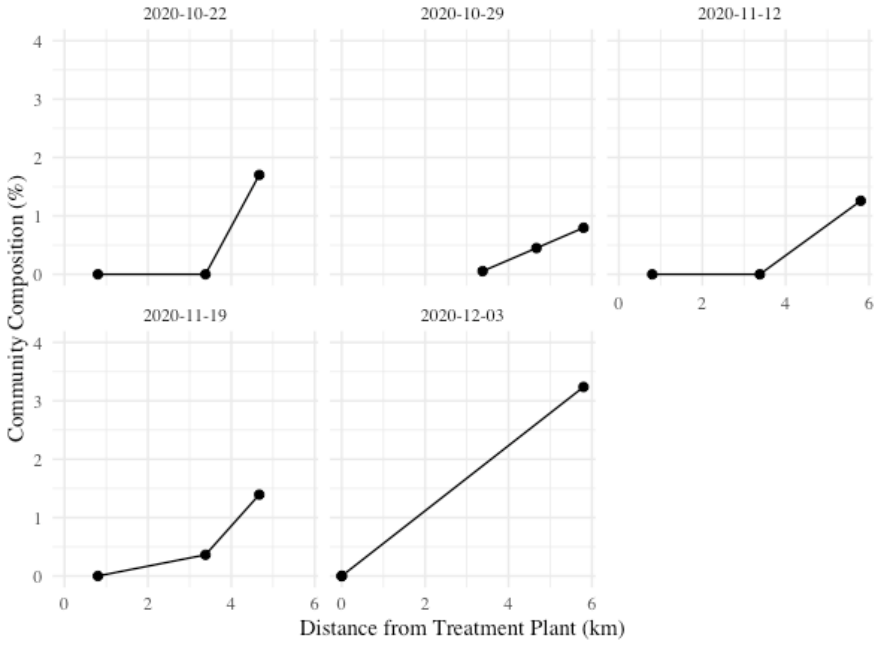

Figure 11: Scatter plot of the summed average relative abundance of the Order Sphingomonadales, and the genera, Nitrospira, Mycobacterium, and Hyphomicrobium. across distance on the dates on which the three taxa increased.

Like the cell concentration measurements, the diversity measurements suggest that the biofilm is not in steady state with the flowing water, i.e., microbes do not enter the flowing water from the biofilm at a constant rate. Instead, stochastic processes, such as biofilm sloughing, appear to influence the microbial community.

16S rRNA gene, Community Characterization

Next, the taxonomic data were analyzed: Examining all phyla detected across all samples, the community composition of samples represents typical phyla associated with planktonic tap water (fig. 12).

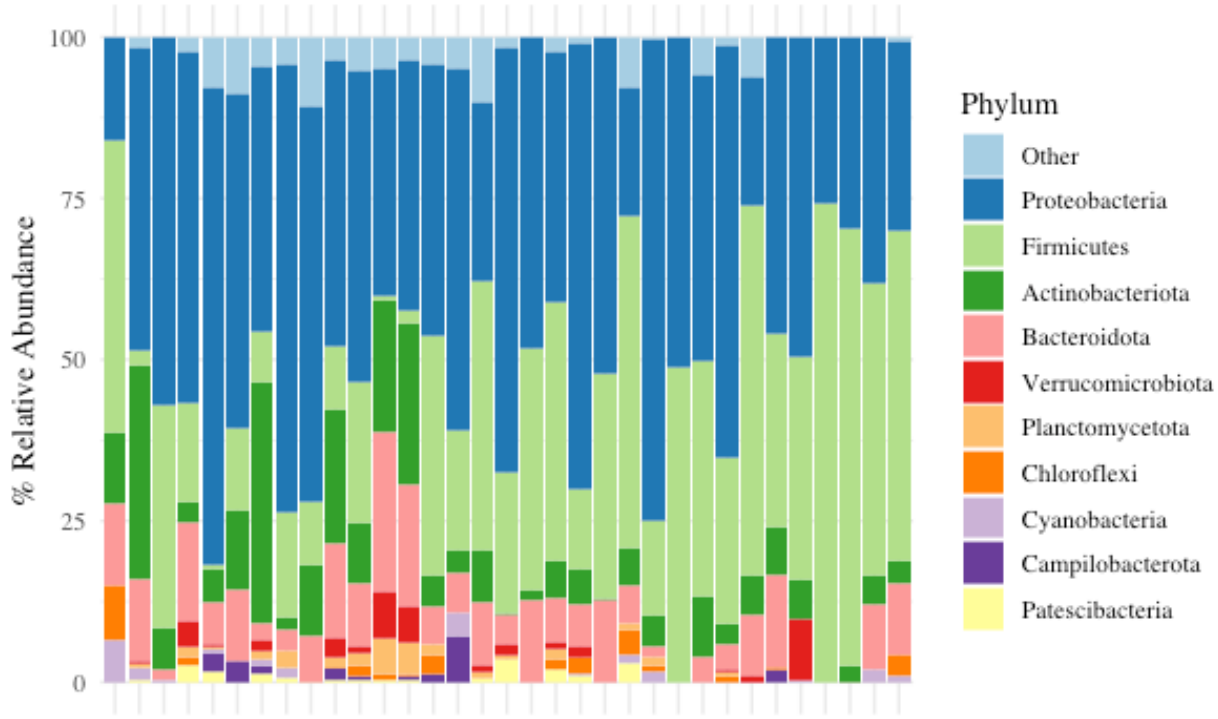

Figure 12: Bar chart of the top ten phyla across all processed samples.

Garner (2008) found similar phyla composition in the drinking water of six treatment plants on the Eastern Coast of the US (Garner et al. 2018). *Proteobacteria, Firmicutes,* and *Actinobacteria* are all common phyla in Lake Michigan, suggesting that these phyla originated from the source water. *Bacteroidota, Verrumicrobia* and *Patescibacteria* are often symbionts and/or parasites of other microbes, which are commonly found in biofilms. To test if communities varied significantly between stations, a multiple analysis of variance (MANOVA) was used. The results of the MANOVA ($f_{3,25} = 0.95$, $p = 0.59$) suggest that distance from the treatment plant alone is not a driver of microbial community in this system (fig. 13). In a similar study, El-Chaktoura (2018) also found that microbial communities did not vary as a function of collection location (El-Chakhtoura et al. 2018).

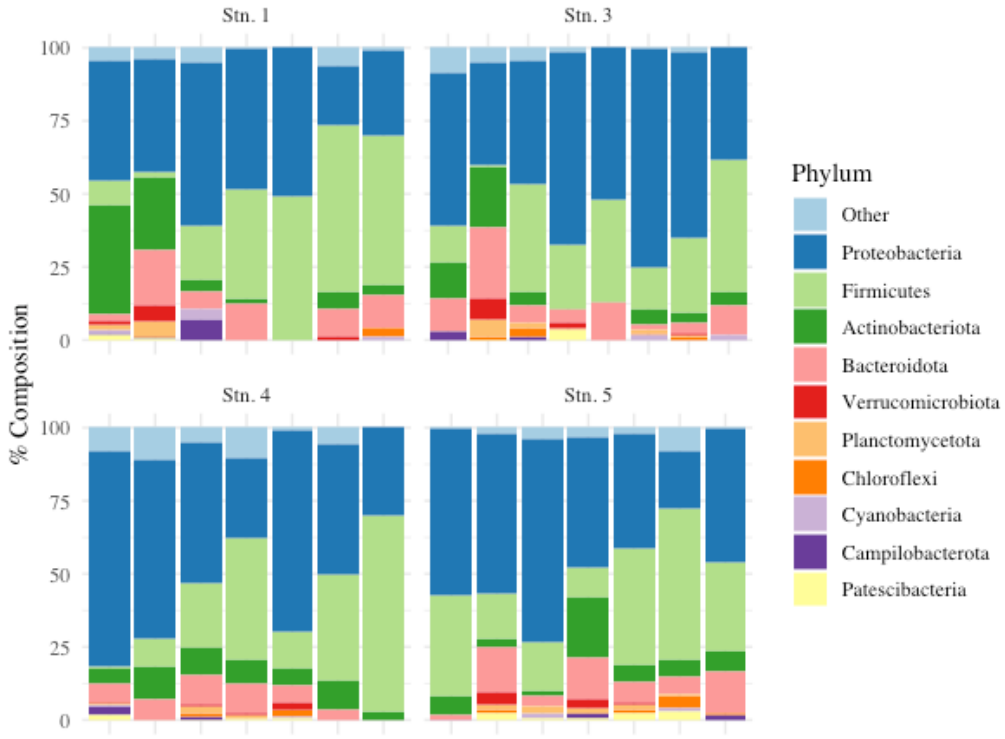

Figure 13: Bar charts of the relative abundance of the top ten phyla by station The result of the MANOVA test for composition difference between the four field stations was not significant, ($f_{3,25}$ = 0.95, p = 0.59); therefore, the community composition does not vary significantly from station to station. The result of the MANOVA test for composition difference between the four field stations and the treatment plant was significant, ($f_{1,31}$ = 1.66, p = .03); therefore, the community within the treatment plant was significantly different from the field stations.

Communities found in distal stations were, however, significantly different from communities found in the treatment plant ($f_{1,31}$ = 1.66, p = 0.03), suggesting that considerable community alterations occur within the flowing water. To determine which taxa were significantly correlated to the treatment plant, the r package *indicator species* was used, which assigns an indicator value to measure the association between a taxa and a location (De C´aceres 2020). The taxa most closely associated with the treatment plant were four members of the phylum *Firmicutes*, common in mature biofilms, three members of the order *Burkholderiales*, commonly associated with lake sediment, and the salt-loving *Halomonas* genus.

Some interesting microbes were able to be identified to the genus level. Perchlorate is a break-down product of hypochlorite, the chemical used by the NSWC as a primary disinfectant (Stanford et al. 2011). Although representatives from diverse phyla have been shown to reduce perchlorate, members of the *Dechloromonas* genus within the *Betaproteobacteria* are the best

studied. Surprisingly, the *Dechloromonas* are beginning to be found more frequently in environmental samples, even in pristine sites with no detectable perchlorate. *Rhodanobacter thiooxidans* is another microbe that feeds off the chemicals used during the treatment plant. Lee et al. first isolated the species from a wastewater biofilter in 2007 (Lee et al. 2021). It is unique in that it can reduce nitrate to nitrite and can oxidize sulfate species to sulfate in the presence of oxygen. Sulfate is added at the treatment plan in the form of alum during the coagulation step.

16S rRNA gene, Core Community

Many previous tap water studies have found evidence of a core community of microbes whose abundance is relatively stable (El-Chakhtoura et al. 2015; W. Li et al. 2018). The core community in this study was determined by isolating those OTUs in both the third quartile of abundance and prevalence. The core community comprised 12.59% of Total OTUs, and composed, on average, 57% of the community abundance. Similarly, El-Chakhtoura (2015) found that across 156 samples in a Swedish drinking water system 58% of OTUs constituted 87% of the community abundance. In the same study, the core microbiome was composed of mainly the phylum, *Proteobacteria*, with the most common classes therein being *alpha*, *gamma*, and *betaproteobacteria*.

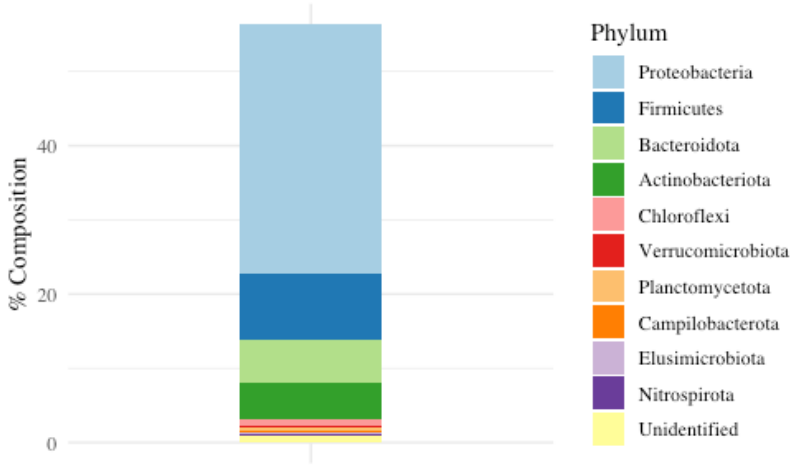

Figure 14: The relative composition of the phyla found in the core community.

The core community in this study was similar to that of the El-Chakhtoura study, except no *gammaproteobacteria*, which are uncommon in Lake Michigan, were present (fig. 14) (Newton et al. 2011). The most common family within the core community were the *Xanthobacteraceae*,

which are aerobic chemoheterotrophs commonly found in freshwater (Oren 2014). The second most common family was the *Gallionellaceae,* which are aerobic ferrous iron-oxidizing bacteria commonly found in pipe scale (Hallbeck and Pedersen 2014; Kimbell et al. 2021). The third most common family was the *Chitinophagaceae,* which are spore-forming facultative anaerobes, some of which can degrade cellulose and chitin (Rosenberg 2014). The fourth and fifth most common were the *Oxalobacteraceae,* which are heterotrophic aerobes and the *Bacilliaceae* which are saprophytic aerobes (Baldani et al. 2014; McBride and Turnbull 1998).

Many members of the core community are common in Lake Michigan, suggesting that these microbes pass through the treatment plant. Because 16S sequencing does not differentiate between live and dead cells, the organisms identified may have originated from deactivated microbes, e.g., microbes whose cell wall has been destroyed. In future experiments, culture-based methods could be combined with 16S data to determine the extent to which the core microbiome is composed of live cells.

qPCR, Legionella

Legionella is a genus of pathogenic microbes that is becoming increasingly indicated in respiratory infections. It is commonly found in stagnant drinking water, and, may become aerosolized in shower heads, or A/C systems. Upon inhalation, *Legionella* may begin to rapidly multiply in immunocompromised hosts and result in acute lung infections which may be fatal if not treated quickly (Bitton 2014). In this study, the quantity of *Legionella* was determined using qPCR. The samples were loaded into StepOne Plus qPCR machine (Life Technologies) and the cycling conditions were as follows: 10 min at 95°C, followed by 40 cycles of 95°C for 15 s, 63°C for 110 s.

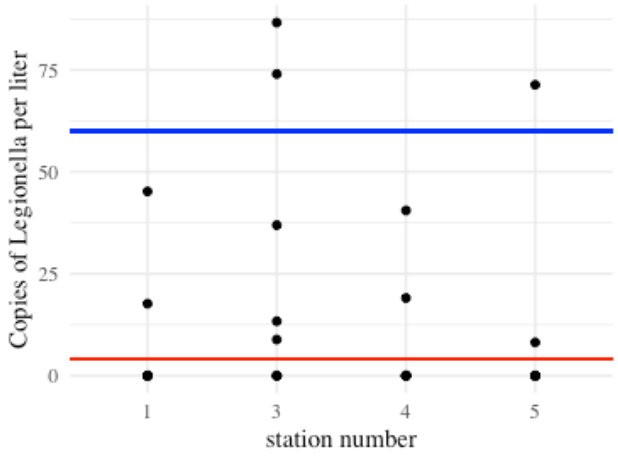

Figure 15: Scatterplot of Legionella copies per liter (determined by qPCR) by station number. The limit of detection, the red line, was 5 copies L^{-1}, the limit of quantification, the blue line, was 60 copies L^{-1}.

No precise correlation between distance from the treatment plant and *Legionella* concentration was deduced. *Legionella* often revert to a dormant state in the biofilms and their concentrations can vary significantly in flowing water due to slight fluctuations in key nutrients (Garner et al. 2018). *Legionella* are also common endosymbionts within amoeba, and they may only emerge from their host under specific conditions (Lienard et al. 2017). Again, stochastic processes seem to exert the most influence over microbial growth in flowing drinking water.

Conclusion:

The evidence presented in this chapter have depicted a largely stochastic nature of microbial communities in flowing water. Distance alone does not seem to impact the cell concentration nor the diversity of microbial communities. This may be because the pipe system is arranged in a series of loops; and therefore water follows a non-linear route as it radiates outwards from the treatment plant. The water age data, therefore, may have a more appreciable impact on community composition than linear pipe-distance data alone. In the next chapter, the procedure for using radionuclides to age water is described in detail, and the resulting water age estimates are analyzed. Then, in the final chapter, the way in which the microbial community changes seasonally, and with retention time, and water chemistry is explored.

CHAPTER 3 – DETERMING WATER AGE USING RADIOMETRIC TRACERS

Introduction:

Water age has been shown to be positively correlated with DBPs, which are negatively associated with human health (Mukundan and Van Dreason 2014). The correlation of water age to microbial community composition is less clear; some studies show younger water ages harboring more diverse communities than older ones; whereas, others show the converse (Wang et al. 2014; A. J. Pinto, Xi, and Raskin 2012). Higher water ages also seem to produce higher microbial loads (Nescerecka et al. 2014). Current research suggests that water age is a key component of both disinfectant decay, and microbial growth; however, a simple, inexpensive water aging method has yet to be developed. Radionuclides may offer a promising means by which to empirically measure water age: indeed, environmental radionuclides have been used to model the transport rates and residence times of a variety of substances in aquatic systems (Moore 1996; England and Maier-Reimer 2001).

Because radioisotopes decay at a known rate, by comparing the activity of a radionuclide at one point in a distribution system to a point downstream, the travel time of water between the two locations may be calculated. Waples et al. (2015) found that the daughter/parent radionuclide pair, $^{90}Y/^{90}Sr$ can be used to accurately measure water age up to 9 days old (σest.: ± 3.8 h, $P < 0.0001$, $r^2 = 0.998$, n = 11) (Waples et al. 2015). Their results were generally consistent with the water ages derived from a hydraulic model for the NSWC.

In this study, the same $^{90}Y/^{90}Sr$ radionuclide pair was selected to measure water age for the following reasons:

1. ^{90}Sr is present at a concentration of about 0.47 dpm L^{-1} in Lake Michigan as a result of atmospheric nuclear weapons testing that occurred throughout the 1960s (Feely, Herbert et al. 1978).

2. ^{90}Sr is generally non-reactive in natural waters (K_d [mL g^{-1}]: $\sim 1 \times 10^2$), and is not removed during drinking water filtration processes; whereas its daughter, ^{90}Y, is particle reactive (K_d: $\sim 1 \times 10^5$), and is removed during water treatment (Joshi 1991; Waples and Orlandini 2010)

3. Relative to its daughter, ^{90}Y (half-life, 64 h), ^{90}Sr is long-lived (half-life, 28.8 yrs); therefore, ^{90}Y grows into equilibrium with ^{90}Sr after about two weeks (Waples and Orlandini 2010).

4. Because ^{90}Sr is nonreactive, its activity is spatially uniform throughout the drinking water pipe system. Likewise, because ^{90}Sr is also long-lived, its activity was essentially constant throughout the four-month study period.

Due to the above characteristics of ^{90}Y/^{90}Sr, the following scenario is hypothesized to occur within the NSWC system. Water containing both ^{90}Y and ^{90}Sr enters the treatment plant from Lake Michigan. During the coagulation step of the treatment process, all the particle-bound ^{90}Y was assumed, and later confirmed (see *Results, Field Samples*), to be removed from the flowing water, leaving only its parent, ^{90}Sr. As ^{90}Sr flows through the pipes, it decays into ^{90}Y at rate determined by its half-life. Specifically, if the change in ^{90}Y activity over time is dominated by the radioactive decay of its parent (and other processes which can affect ^{90}Y activity – including advective and diffusive fluxes, scavenging to the pipe wall, or resuspension from the pipe wall – are negligible), then the change in ^{90}Y over time can be expressed as:

$$Y_2 = \frac{\lambda_Y Sr}{\lambda_Y - \lambda_{Sr}}\left(e^{-\lambda_{Sr}t} - e^{-\lambda_Y t}\right) + Y_1\left(e^{-\lambda_Y t}\right) \quad (1)$$

where *Sr* and *Y* are activities of ^{90}Sr and ^{90}Y, λ is the decay constant for ^{90}Sr (6.5916×10^{-5} day^{-1}) or ^{90}Y (0.25993 day^{-1}), subscripts *1* and *2* relate to initial and subsequent sampling periods, and *t* is the time interval between sampling (Waples et al. 2015). Moreover, because the half-life of ^{90}Y is much shorter than that of ^{90}Sr (i.e., $\ll 1\%$), equation 1 can be simplified and rearranged to solve for *t*, so that the ^{90}Y activity measured at any point in the pipe system is related to the *water age* via the following equation,

$$water\ age = \frac{\ln\left(\frac{A_{90SrM} - A_{90Ycl}}{A_{90SrM} - Y_{90Ytp}}\right)}{\lambda_{Y90}} \quad (2)$$

where, A_{90SrM} is the ^{90}Sr activity within the system; A_{90Ycl} is the ^{90}Y activity at a point distal to the treatment plant; A_{90Ytp} is the ^{90}Y activity at the treatment plant; and, λ_{Y90} is the constant, 0.2596325963 days^{-1}. According to this conceptual framework, the ^{90}Sr activity throughout the system, and the ^{90}Y activity at a sampling location can be used to calculate water age at any point along the distribution system. The following overview outlines the methodology to determine the

activities of both ^{90}Sr, and ^{90}Y; and, to verify the accuracy of the water aging protocol. The protocol is then described in greater detail in the following sections.

Methods, Overview:

The concentration of ^{90}Sr in the pipe system was determined by measuring ^{90}Y, after it had grown into secular equilibrium with its parent. Because ^{90}Y has a half-life much smaller than that of ^{90}Sr, within a closed system, after five ^{90}Y half-lives (~2 weeks), the activity of ^{90}Y equilibrates to the activity of ^{90}Sr, i.e., ^{90}Y reaches secular equilibrium with its parent..

To determine the ^{90}Sr activity in the study system, six water samples were collected on 7/16/20 at a tap in the SFS building. The six samples were acidified to a pH of ~1 using concentrated HCl to prevent ^{90}Y from adsorbing to the plastic walls of the carboy. Immediately afterwards, a known activity of ^{88}Y was added to the sample as a yield monitor. ^{88}Y was assumed to behave exactly as ^{90}Y during the sample processing. The samples were then incubated for 2 weeks. Iron sulfate was added to the sample. Then the sample was alkalized to a pH of ~10 to precipitate the iron, to which the particle-reactive yttrium (i.e., ^{90}Y and ^{88}Y) formed a bond. The yttrium was then isolated from each of the samples in two separation steps.

In the first step, the sample was filtered onto a 0.45 µm filter. The precipitated iron, together with the bound yttrium remained on the filter; whereas, ^{90}Sr passed through the filter, because it is not particle reactive. The ^{90}Y, now separated from its parent, no longer grew into the system. During the second filtration step, the ^{90}Y and ^{88}Y isotopes were isolated from most other beta-emitters on an anion exchange column (some beta emitters, notably ^{212}Pb, remained, see figure A1).

The rate of ^{90}Y decay was measured using a beta counter and the counts of beta particle emissions were used to back-calculate (forecast backward) the activity of ^{90}Y at the time of the initial filtration step. The recovery of ^{90}Y was determined by comparing the known activity of ^{88}Y added to the sample to its measured activity after all processing steps. Because ^{88}Y emits gamma energy upon its decay, after the sample was counted for beta emissions, it was counted again in a gamma detector. The activity of ^{90}Y in the sample at the time of filtering was then calculated from the beta count data, and subsequently corrected by the recovery of ^{88}Y. Because

^{90}Y had grown into secular equilibrium with ^{90}Sr by the time the sample was filtered, the ^{90}Y activity was equivalent to the ^{90}Sr activity.

After determining the starting activity of ^{90}Sr in the system, field sampling commenced. Water age samples were collected concurrently with microbiology samples: samples were collected from four hydrants within the Whitefish Bay distribution system of the North Shore Water Commission throughout the fall of 2020. Field samples were processed similarly to the incubated samples to determine the activity of ^{90}Y at the time of sampling. After processing the data, equation 2 was used to determine the water age of each sample. The water age was then compared to the microbiological data to assess trends in microbial populations with increasing retention time in the distribution system (see chapter 4).

To evaluate the accuracy of the water-aging protocol, a time series experiment was conducted. Five samples collected from a tap in SFS on 3/17/21 were processed subsequently in 24-hour intervals. The same water aging methods used for the field methods was used to determine the length of time elapsed from the first filtration of the first sample in the series, to the first filtration of each of the subsequent samples in the series, the "relative water age." The relative water age was then compared to the known elapsed time between filtering (~24 hours) using a simple linear regression.

Methods, ^{90}Sr Experiment, Sample Collection:

On 7/16/20, a tap in the SFS building was opened and allowed to run for ten minutes, then six 20 L carboys were filled. Each carboy was acidified to a pH of ~1 using concentrated HCl, and then allowed to incubate for two weeks. This allowed the ^{90}Y to grow into equilibrium with its parent ^{90}Sr.

Methods, Field Experiment, Sample Collection:

From August through December of 2020, the Glendale Water Treatment Plant and four hydrants in the Whitefish Bay distribution network were monitored (fig. 1). Assuming water exiting the plant traveled along the shortest possible existing pipe route to each station, the distance from the plant to the hydrants was as follows,

Table 2: Station location and number of times sampled for water age..

Station name	Address (in Whitefish Bay, WI)	Distance from treatment plant (km)	Times sampled for water age.
Treatment Plant	400 W Bender Rd (Glendale, WI)	0	1
1	6142 N Lydell Ave	0.81	6
3	902 E Lexington Avenue	3.38	6
4	1100 E Courtland Pl	4.67	6
5	4524 N Frederick Ave	5.80	5

Samples were collected between 8 and 10 am on a weekly basis, for a complete list of the dates on which radiochemistry samples were collected, see table A2. At each station, the hydrant was opened and flushed for approximately five minutes, until the water was visibly clear. Then, two 20 L plastic carboys were filled and immediately acidified to a pH of ~1 using concentrated HCl. The samples were transported back to SFS and the following daughter counting procedure was performed as soon as possible.

Methods, Counting ^{90}Y and ^{88}Y:

In the lab, each sample received 2 ml of ~30 dpm ml^{-1} ^{88}Y (Eckert & Ziegler Isotope Products), which was used as a yield monitor; 10 mg of ferrous iron (added as a ferrous sulfate solution); and, 4 ml of a ^{88}Sr hold-back solution (Waples and Orlandini 2010). Concentrated ammonium hydroxide was then added to the sample to raise the pH to ~10. This created an iron precipitate, which scavenged the yttrium in the sample. The sample was then filtered to collect the iron precipitate onto a nitrocellulose filter (0.45 µm, 293 mm, Millipore). At this point, the ^{90}Y was completely separated from its parent, ^{90}Sr.

Next, the filter was folded, cut into pieces, placed in a beaker, and covered with 50 ml of 1 M HCl. The filter was crushed using a glass stir bar to dissolve the iron, and the HCl-Fe solution was filtered through an anion exchange column to isolate the ^{90}Y from ^{210}Bi – another short-lived (5.0 day half-life) beta emitter that could have interfered with the interpretation of beta counts from ^{90}Y decay. Columns were prepared using an anion exchange resin (Bio-Rad. AG50W-X8, 100 – 200 mesh) and glass Pasteur pipettes. After eluting the sample through the column, the column was washed with 1 M HCl.

The eluted solution was then combined with a few drops of 12 M ammonium hydroxide to precipitate the dissolved iron. The solution was then filtered on to a nitrocellulose filter (0.45 µm, 17 mm, Millipore). Then, the filter was dried and glued to a cupped stainless steel planchet (2 inches diameter, A. F. Murphy Die and Machine Co.). Beta counting of the dried filter was conducted using a low background gas-flow proportional counter with 2.25-in.-diameter detectors and anti-coincidence circuitry (G542 System, Gamma Products). Beta counts were run in 150-minute intervals over a period lasting up to several weeks. Due to the decay of the short-lived isotope, ^{212}Pb (half-life, 10.64 h), the first 2.5 days of beta counts were removed from the analysis on every sample, except incubated samples (samples filtered >2.5 days after collecting). Similarly, due to the decay of long-lived isotopes, such as ^{234}Th (half-life, 24.1 days) counts measured >8.5 days after the initial beta count were removed. The counts were then processed to determine the ^{90}Y activity at the time of filtering (see calculation example below).

After beta counting, the filter was removed from the steel planchet and rolled into a 2 ml tube. The tube was capped and placed into a Canberra gamma spectroscopy system with an HPGe well detector (model GCW 4023) to determine ^{88}Y recovery. Gamma counts with an energy of 897 keV were measured for approximately 250,000 seconds.

Example Calculation, Percent Recovery:

The recovery of the ^{88}Y yield monitor was assumed to be equivalent to the recovery of ^{90}Y in the sample. The following equations were used to determine the ^{90}Y recovery: the data for a field sample, tap30, are used as an example. Sample data collected directly from both the gamma and the beta counters are ascribed the units of *disintegrations (dsn).* The data necessary to determine the ^{88}Y recovery in this example field sample are outlined in the following table:

Table 3: Data necessary to calculate the recovery of ^{88}Y Yield Monitor

Parameter Name	Description	Value
A_{88Y0}	^{88}Y yield monitor stock solution specific activity determined by its manufacturers, Eckert & Ziegler Isotope Products (EZIP).	282.27 dpm ml^{-1}

T_s	Date on which EZIP measured the ^{88}Y activity.	11/1/19
V_{88Y}	Volume of ^{88}Y standard added to the sample.	2 ml
T_{cl}	Time of sample collection at the hydrant.	9/1/2020 9:34
T_f	Time of the first filtration step, at which ^{90}Y was isolated from ^{90}Sr.	9/1/2020 15:20
C_{88Y}	897 keV area of the gamma counter output: ^{88}Y emits energy mostly in this range.	6010 dsn
C_{88Ye}	The error associated with the ^{88}Y gamma count.	90.81 dsn
T_l	The duration of gamma counter measurement.	2.03 days
E_{gc}	The average efficiency of the gamma counter for ^{88}Y, i.e., gamma counts/disintegrations.	0.06963
EgcE	The standard deviation of gamma counter efficiency.	7.8E-4

The yield monitor activity was measured by its manufacturers on 11/1/19. To determine the activity of the ^{88}Y yield monitor added to the sample at the time of sample processing, $N_{Y88,}$ the exponential decay equation was used:

$$N_{Y88} = (V_{Y88} * A_{88Y0})e^{-\lambda_{88Y}T_{gc}} \quad (3)$$

Where λ_{88Y} is the natural log of 2 divided by the half-life of ^{88}Y, $t_{½\ 88Y}$

$$\frac{\ln(2)}{t½_{88Y}} = \lambda_{88Y} = \frac{0.69}{106.63\ days} = 0.0065\ days^{-1} \quad (4)$$

and, T_{gc} is the time elapsed between the day on which the ^{88}Y standard was measured, T_s, and the day on which the ^{88}Y was added to the sample, T_{cl}.

$$T_{cl} - T_s = T_{gc} = 9/1/2020 - \ 11/1/19 \ = \ 407 \ days \tag{5}$$

Substituting (4) and (5) into (3), the activity of the 2 ml of yield monitor, N_{Y88}, added to the sample was calculated,

$$(2 \ ml * 287.27 \ dpm \ ml^{-1}) * e^{0.0065 \ days^{1} * 407 days} \ = N_{Y88} = 39.89 \ dpm \tag{6}$$

If the efficiency of the gamma detector was 100% and the entire volume of ^{88}Y added to the sample in the beginning of the filtering process was present on the final filter, then the gamma counter would measure, 39.89 dpm. However, because, 1) the gamma detector efficiency for ^{88}Y is only ~7%, 2) some ^{88}Y was inevitably lost during the processing steps, and, 3) some ^{88}Y decayed during the counting process, the actual activity of ^{88}Y measured on the final filter was lower. The next calculation steps correct the reading of the gamma counter for the ^{88}Y decay that occurred during the 2.03 days of counting, and the imperfect ^{88}Y counter measuring efficiency.

The live time, T_l, of the gamma counter is the duration for which the counter was actively measuring gamma radiation. Because ^{88}Y was actively decaying during the count, the following equation was used to correct for the decay of ^{88}Y while the sample was being counted, T_{lCtd}.

$$\frac{\lambda_{88Y} T_l}{1 - e^{-\lambda_{88Y} T_l}} = T_{lCtd} = \frac{0.0065 \ days^{-1} * \ 2.03 \ days}{1 - e^{-0.0065 \ days^{-1} * 2.03 \ days}} = 1.066 \tag{7}$$

The sample decay correction factor was then multiplied by the number of gamma counts measured during the ^{88}Y detector live time to determine the number of disintegrations that would have been measured had no ^{88}Y decay occurred during the counting process, C_{88Yctd}.

$$T_{lCtd} * C_{88Y} = \ C_{88Yctd} = 1.066 \ * 6010 \ counts = 6049.83 \ dsn \tag{8}$$

The error associated with the disintegration measurement also needed to be corrected by the correction factor,

$$C_{88Ye} * T_{lCtd} = C_{88YeCtd} = 90.81 \ counts * 1.066 \ = 91.41 \ dsn \tag{9}$$

The corrected number of disintegrations measured was divided by the number of expected disintegrations to determine the gamma counter recovery efficiency, R_E, for this sample:

$$\frac{C_{88Yctd}}{T_l * E_{gc} * N_{Y88}} = R_E = \frac{6049.83\ dsn}{2929.37\ minutes * 0.06963 * 39.89\ dpm} = 0.744 \qquad (10)$$

To propagate the errors associated with the disintegration measurements and the gamma counter recovery, R_{Ee}, the following equation was used,

$$R_E\left(\left(\frac{E_{gcE}}{E_{gc}}\right)^2 + \left(\frac{C_{88YeCtd}}{C_{88Yctd}}\right)^2\right)^{.5} = R_{Ee} = 0.744\left(\left(\frac{7.8E^{-4}}{0.7}\right)^2 + \left(\frac{91.41\ dsn}{6049.83\ dsn}\right)^2\right)^{.5} = 0.014 \qquad (11)$$

For tap30, the recovery of ^{88}Y was 0.744 ± 0.014.

Example Calculation, ^{90}Y Activity at Time of Sampling:

If the recovery of ^{88}Y determined above was equivalent to the recovery ^{90}Y, then both the activity of ^{90}Y at the time of filtering and at the time of sampling can be determined by performing the calculations outlined below. The following table describes the data necessary to determine the ^{90}Y activity for tap30, the same field sample used in the above example,

Table 4 Data necessary to calculate the recovery ^{90}Y at time of sampling.

Parameter Name	Description	Value
T_f	The time at which the sample was filtered to separate ^{90}Sr from its daughter, ^{90}Y.	9/1/2020 15:20
T_{ct}	The time of the start of a 150-minute beta counting interval.	Various
T_{cl}	Time of sample collection at the hydrant.	9/1/2020 9:34
R_E	The fraction of ^{88}Y recovered after all processing steps, determined in the previous section.	0.744
R_{Ee}	The error associated the $R_{E,}$ determined in the previous section.	0.014
E_{bc}	The efficiency of the beta detector, i.e., the fraction of beta emissions released counted by the detector.	0.495
E_{bcE}	The error associated with E_{bc}.	0.0284
V_s	The volume of drinking water taken from the hydrant.	27.22 L
A_{90SrM}	The mean ^{90}Sr activity, as determined by the six incubated samples, see below.	0.47 dpm L^{-1}

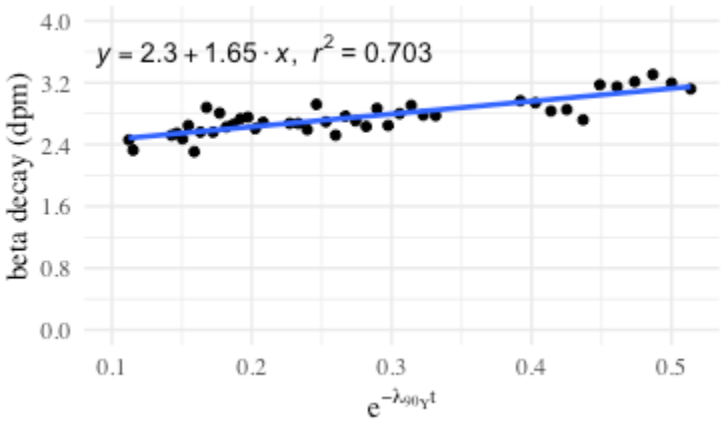

Figure 16: Beta decay of tap30 plotted by the ^{90}Y decay function, $e^{-\lambda_{Y90}t}$, where λ_{90Y} is 0.00018 mins^{-1} and t is the time elapsed from the beginning of the 150 minute beta count read interval to the time of filtering. Decays measured <2.5 days after filtering were removed due to the influence of short-lived radioisotopes (^{212}Pb). Decays from >8.5 days after filtering were removed due to the influence of long-lived radioisotopes (^{234}Th). A simple linear regression equation is shown on the chart.

The beta counter operated in 150-minute intervals. For each counting interval, the beta counts per minute were derived by dividing the total number of beta counts measured by 150 minutes. On average, each sample was measured for 107 intervals. After removing counts taken <2.5 days after the initial filtration step, and >8.5 days after the initial filtration step, the ^{90}Y decay at the time of filtration, C_{90Y0}, was derived from the following linear regression formula,

$$C_{90Y} = C_{90Y0} * e^{-\lambda_{Y90}T_{FS}} \quad (12)$$

Where C_{90Y0} are the counts per minute data from the beta counter. And where T_{FS} is the time elapsed from the initial filtration step, T_f, to the time of the start of the counting interval, T_{ct}. After computing the simple linear regression, all points for which the absolute value of the standardized residual was greater than 3 were deemed outliers and removed from the data. The regression was then re-evaluated with only the non-outlying data points (fig. 16). The modelled slope of the regression equation, $C_{90Y0,}$ ± its associated standard error, C_{90Y0e}, was 1.653 ± 0.168 dpm.

Next the slope was corrected by both the ^{90}Y recovery efficiency, R_E, and the beta detector efficiency, E_{bc}.

$$\frac{C_{90Y0}}{R_E E_{bc}} = N_{90Y0} = \frac{1.653\ cpm}{0.744 * 0.495} = 4.49\ dpm \quad (13)$$

To propagate the error associated with the linear regression, the ^{88}Y recovery efficiency, and the detector efficiency, the following equation was used,

$$N_{90Yf}\left(\left(\frac{C_{90Y0e}}{C_{90Y0}}\right)^2 + \left(\frac{R_{Ee}}{R_E}\right)^2 + \left(\frac{E_{bcE}}{E_{bc}}\right)^2\right)^{.5} = N_{90Yfe}$$

$$= 4.49\ dpm\left(\left(\frac{0.168\ cpm}{1.653\ cpm}\right)^2 + \left(\frac{0.014}{0.744}\right)^2 + \left(\frac{0.0284}{0.495}\right)^2\right)^{.5} = 0.53\ dpm \quad (14)$$

Then, to determine the activity of ^{90}Y per liter of sample at initial filtration step, A_{90Yf},

$$\frac{N_{90Yf}}{V_s} = A_{90Yf} = \frac{4.49\ dpm}{27.22L} = 0.16\ dpm\ L^1 \quad (15)$$

To propagate the error of the ^{90}Y activity, the following calculation was performed,

$$\frac{N_{90Yfe}}{V_s} = A_{90YfE} = \frac{0.53\ dpm}{27.22\ L} = 0.02\ dpm\ L^1 \quad (16)$$

NB. For the incubated samples, the activity of ^{90}Y at the time of filtration was used as a proxy for the ^{90}Sr activity per liter of sample. The following equations were calculated only for the field samples.

To back-calculate the activity of ^{90}Y at the time of sample collection, the following procedure was performed. The time elapsed from sampling, $T_{cl,}$ to the initial filtration step, T_f was calculated,

$$T_f - T_{cl} = T_e = 9/1/2020\ 15{:}20 - 9/1/2020\ 9{:}34 = 0.14\ days \quad (17)$$

Then, the following equation was used,

$$\frac{[A_{90Yf} - (\lambda_{90Y}/(\lambda_{90Sr} - \lambda_{90Y})) * A_{90SrM} * (e^{-\lambda_{90Sr}T_e}) - (e^{\lambda_{90Y}T_e})]}{(e^{-\lambda_{90Y}T_e})} = A_{90Ycl} =$$

$$\frac{[0.16\ dpm\ L^{-1} - (0.260\ days^{-1}/(\ 6.57E{-}5\ days^{-1} - 0.260\ days^{-1})) * 0.47\ dpm\ L^{-1}}{\left(e^{-0.260 days^{-1} * 0.14\ days}\right)} *$$

$$\frac{(e^{-6.57E5\ days^{-1}*0.14\ days}) - (e^{-0.260\ days^{-1}*.014\ days})]}{\left(e^{-0.260\ days^{-1}*0.14\ days}\right)} = 0.15\ dpm\ L^{-1}$$

(18)

Then, to propagate the error associated with the ^{90}Y concentration at the time of filtering, the following equation was used,

$$\frac{A_{90Ycl}}{A_{90Yf}} * A_{90YfE} = A_{90YclE} = \frac{0.15\ dpm\ L^{-1}}{0.16\ dpm\ L^{-1}} * 0.02\ dpm\ L^{-1} = 0.02\ dpm\ L^{-1} \qquad (19)$$

Results, ^{90}Sr Experiment:

Before calculating the water ages of the field samples, the ^{90}Sr activity needed to be derived from the incubated samples. Because ^{90}Y had grown into secular equilibrium with ^{90}Sr, the ^{90}Y activity of the incubated samples at the time of filtering was equal to the ^{90}Sr activity. After correcting the ^{90}Y beta count data by its recovery, derived from the ^{88}Y gamma energy data, the ^{90}Y activity at the time of initial filtration was determined for all the incubated samples using the above calculations.

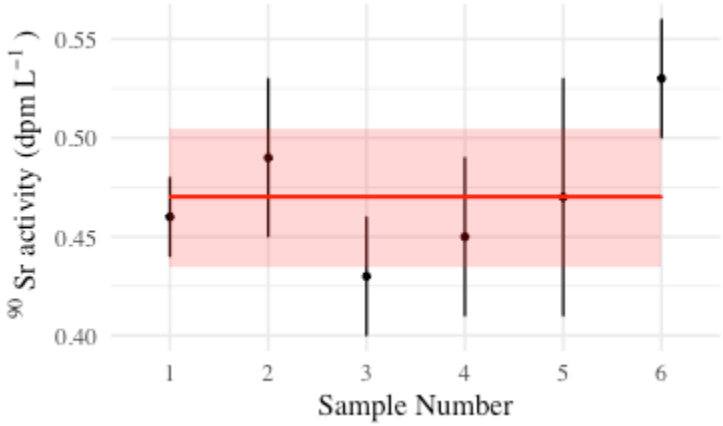

Figure 17: Scatter plot of ^{90}Sr activity after two weeks of sample incubation, n = 6 replicates. The mean ^{90}Sr activity ± the standard error of the mean was 0.47 ± 0.04 dpm L^{-1} (n = 6, ±1 SD): the red line is the mean, and the red box bounds the standard error of the mean.

The ^{90}Sr activity in samples collected from the School of Freshwater Sciences (Tap samples 1-6) was 0.47 ± 0.04 dpm L^{-1} (n = 6, ±1 SD) (fig. 17). This was assumed to equal the ^{90}Sr activity in the NSWC distribution system and later confirmed with an aged water sample from the NSWC system: an incubated sample collected on 4/28/21 yielded an ^{90}Sr activity of 0.45 ± 0.04 dpm L^{-1}.

Calculation Example, Water Age:

After ascertaining the ^{90}Sr activity in the system, the water age could be calculated from the ^{90}Y activity at the time of sampling. The following data was used to determine the water age for the example sample, tap30.

Table 5: Data necessary to calculate water age at time of sampling.

Parameter	Description	Value
A_{90SrM}	The mean ^{90}Sr activity from the 6 incubated samples (fig. 17).	0.47 dpm L^{-1}
A_{90SrMe}	The standard deviation of the mean for the six incubated ^{90}Sr samples.	0.04 dpm L^{-1}
A_{90Ytp}	^{90}Y activity at the treatment plant after the coagulation step.	0 dpm L^{-1}
A_{90YtpE}	^{90}Y activity treatment plant error.	0 dpm L^{-1}
A_{90Ycl}	The ^{90}Y activity at the time of sample collection, derived using the calculations described in the previous section.	0.15 dpm L^{-1}
A_{90YclE}	The error associated with Y_{Acl}, derived in the previous section.	0.02 dpm L^{-1}

Because ^{90}Y grows into the system from its parent ^{90}Sr at a known rate, and the treatment plant theoretically removed all ^{90}Y from the water, the concentration of ^{90}Sr can be compared the concentration of ^{90}Y at any station to determine the time elapsed from sampling to the time of water treatment (the water age). The following equation was used to determine the water age,

where, A_{90SrM} is the parent nuclide activity; A_{90Ytp}, and A_{90Ycl} are the daughter nuclide activities at the treatment plant and station one respectively; and, λ_{Y90} is a constant derived from the half-life of ^{90}Y.

$$\left[-l\,\mathrm{n}\left(\frac{A_{90SrM}-A_{90Ycl}}{A_{90SrM}-A_{90Ytp}}\right)/\lambda_{Y90}\right]*24\ hours = water\ age =$$

$$\left[-l\,\mathrm{n}\left(\frac{0.47\ dpm\ L^{-1}-0.15\ dpm\ L^{-1}}{0.47\ dpm\ L^{-1}-0\ dpm\ L^{-1}}\right)/0.260\ days^{-1}\right]*24\ hours = \ 36.5\ \text{hours} \qquad (20)$$

The water age at time of sampling for this sample was 36.5 hours. The error associated with the water age was derived from the results of the time series experiment described below. Briefly, a series of five samples, incubated for a known period, were aged using the above described technique. The ^{90}Y derived ages were then compared to the known length of sample incubation. A linear regression was fitted to the data, and the standard error of the estimate for the model, $\delta_{est,}$ was the error of the water age for all the field measurements in the study (Waples et al. 2015).

Methods, Time Series Experiment:

To determine the accuracy of the water aging method, five tap water samples were collected from SFS on 3/17/21. The samples were all acidified to a to a pH of ~1 using HCl. Then, one sample was processed for ^{90}Y activity according to the methodology outline above, every ~24 hours for five days. The same calculations for deriving the ^{90}Y activity at the time of filtering described above were performed. The rate of ingrowth of ^{90}Y activity over the five day period was used to estimate ^{90}Sr activity (see below). The $^{90}Y/^{90}Sr$ activity ratios were used to derive a water age, which were then compared to the known sample ages [calculated as the time elapsed between sample collection and sample processing]. The computation steps are outlined below.

Results, Time Series Experiment, ^{90}Sr Estimate:

Because the half-life of ^{90}Sr is much larger than ^{90}Y, the following equation can be used to model the change of ^{90}Y activity from an initial time, A_{90Y0}, to a future time, A_{90YF}, after T_{F0F} time has elapsed.

$$A_{90YF} = (A_{90SrTS} - A_{90Y0}) * \left(1 - e^{-\lambda_{Y90} T_{F0F}}\right) \quad (21)$$

After determining the ^{90}Y activity at the time of filtering for all of the samples in the time series, the left hand side of the equation was plotted against $1 - e^{-\lambda_{Y90} T_{F0F}}$, then a simple linear regression was computed (fig. 18). The estimated slope plus the y-intercept, A_{90Y0}, was the ^{90}Sr activity derived from the time series experiment, A_{90SrTS}.

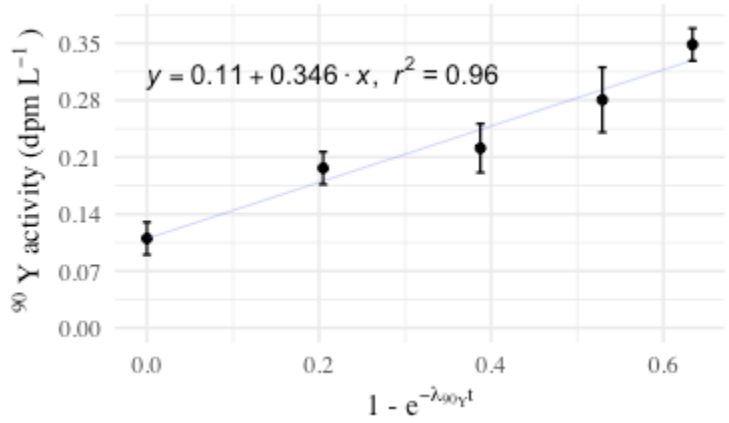

Figure 18: ^{90}Y activity at the time of filtering for the five samples in the time series plotted against $1 - e^{-\lambda_{Y90} T_{F0F}}$. The results of a simple linear regression are shown on the chart.

The slope of the linear regression was 0.346 and the Y intercept was 0.11 (fig. 18). The addition of these parameters yields the time series estimate of ^{90}Sr activity, 0.456 dpm L^{-1}. The associated error was computed as the sum of the uncertainty of the slope plus the uncertainty of the y intercept, 0.058 dpm L^{-1}. The ^{90}Sr activity determined from the incubation experiment, 0.47 ± 0.04 dpm L^{-1} (n = 6, ±1 SD) falls within an acceptable range from the estimate derived from this experiment.

Calculation Example, Relative Water Age:

Using the estimated ^{90}Sr activity, A_{90SrTS}, and the ^{90}Y activity at the time of filtering for the first sample in the sequence, A_{90Y0}, the time elapsed from the first sample filtered to the filtration time of each of the four remaining samples, the "relative water age," was calculated. To determine the relative water age of the second sample in the series, tap45, the following data were used:

Table 6: Data used to calculate the relative water age.

Parameter	Description	Value
A_{90SrTS}	The ^{90}Sr activity determined using the regression outlined in the previous section (figure 18).	0.456 dpm L^{-1}
A_{90Y0}	The ^{90}Y activity at the time of filtering for the first sample in the sequence.	0.11 dpm L^{-1}
A_{90Yts}	The ^{90}Y activity at the time of filtering for the second sample in the sequence.	0.20 dpm L^{-1}

The relative water age was computed using a similar equation to determine the water age of the field samples.

$$\left[-l\,\mathrm{n}\left(\frac{A_{90SrTS}-A_{90Yts}}{A_{90SrTS}-A_{90Y0}}\right)/\lambda_{Y90}\right]*24\ hours = relative\ water\ age$$

$$= \left[-l\,\mathrm{n}\left(\frac{0.456\ dpm\ L^{-1}-0.20\ dpm\ L^{-1}}{0.456\ dpm\ L^{-1}-0.11\ dpm\ L^{-1}}\right)/0.260\ days^{-1}\right]*24\ hours$$

$$= 25.68 \text{ hours} \qquad (22)$$

The time elapsed between the first sample filtered and the second sample filtered was predicted to be 25.68 hours. The actual elapsed time between filtering was 21.15 hours.

Results, Time Series Experiment, Relative Water Age:

After computing the relative water ages for every sample in the time series, the modelled relative water ages were compared to the known relative water ages and a simple linear regression was computed (fig. 19).

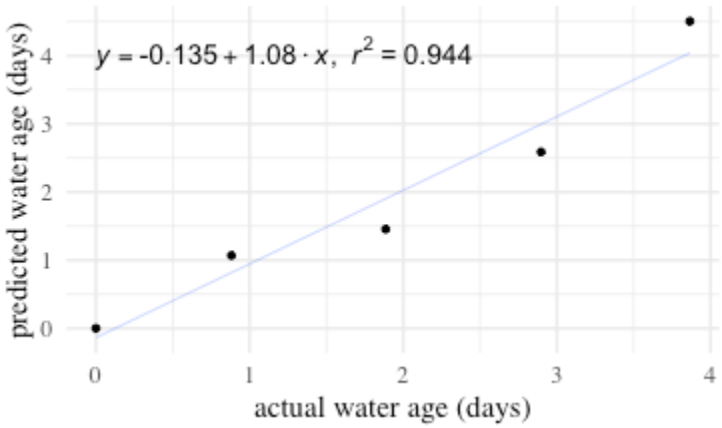

Figure 19: Scatter plot of the actual water age plotted against the ^{90}Y derived water age. A linear regression was fitted to the points, with the equation shown on the chart. The standard error of the estimate of the regression equation, δ_{est}, 10.131 hours.

The standard error of the estimate for the linear model, δ_{est}, was 10.1 hours. This estimate was used as the error for all the water age measurements throughout the study.

Results, Field Samples:

After assessing the accuracy of the ^{90}Y processing protocol, and determining the error of the water age estimates, the results of the field experiment were analyzed. Because the ingrowth of ^{90}Y is constrained by the ingrowth of its parent, ^{90}Sr, the activity of ^{90}Y should never exceed the activity of ^{90}Sr in a closed system; however, the ^{90}Y activity measured at station 1 did exceed the ^{90}Sr activity, as determined in the incubation experiment (fig. 20; table A3).

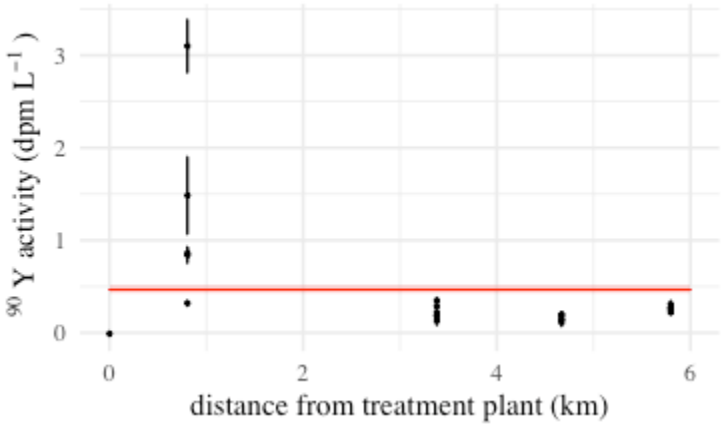

Figure 20: Scatter plot of ^{90}Y activity at time of sample collection against distance from plant on each sampling date. The red line indicates the mean ^{90}Sr activity in the pipe system as

determined by the incubation experiment, the red rectangle bounds the standard deviation of the mean, 0.47 ± 0.4 dpm L^{-1}.

At the first station, ^{90}Y activities greater than the mean ^{90}Sr activity were measured on four separate occasions (fig. 20) (table A3). Because ^{90}Y activity can never be higher than its parent [in a closed system], there are only two possible explanations for the high activities observed. Either (1) ^{90}Sr activity in the station 1 samples must also have been at least as high, or (2) pipe deposits that contained ^{90}Y activity were resuspended into the water stream during the sampling process. Because ^{90}Sr is so long-lived, and ^{90}Y activities decreased to activities below 0.47 dpm L^{-1} by station 3 [on samples collected during the same day], we hypothesize that the high ^{90}Y activities observed at station 1 were associated with particulate matter. The rate of decrease of ^{90}Y activity from stations 1 to 3 and 3 to 4 could have been caused by the radioactive decay, but the observed decrease in activity occurred much too rapidly and ^{90}Y would have plateaued at an activity equal to the previously measured ^{90}Sr activity (i.e., 0.47 dpm L^{-1}).

Under the assumptions used to model the system in this experiment, ^{90}Y grows into the flowing water only from a stable reservoir of ^{90}Sr. Consequently, the activity of ^{90}Y in the flowing water would have increased as the water moved downstream from the treatment plant. In the data collected, the hypothesized ^{90}Y behavior only occurred between stations 4 and 5 (fig. 21B).

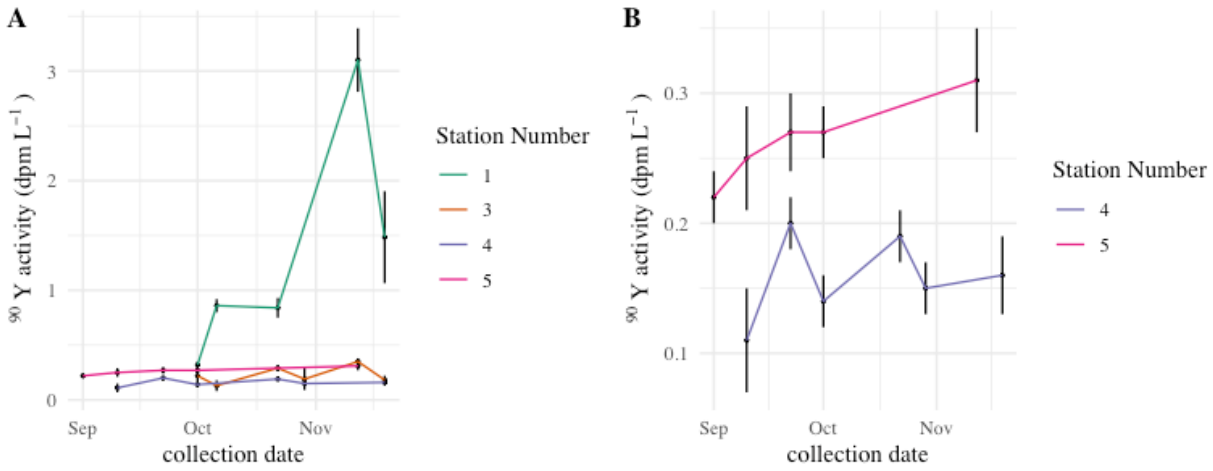

Figure 21: Scatter plot of ^{90}Y activity plotted by date, with all stations delineated (A) and with stations 4 and 5 delineated (B).

The activity of ^{90}Y increases between stations 4 and 5, as expected and we hypothesize that the particulate matter that appeared to influence ^{90}Y activities at stations 1 and 3 had settled out [or become negligible] by station 4. Consequently, water ages were only resolved for stations 4 and 5, yielding the following estimates:

Table 7: Water age data for stations 4 & 5

Sample Name	Station Number	Time Sampled	^{90}Y Activity (dpm L^{-1})	Water Age (hours)
tap13	5	9/1/20 10:17	0.22 ± 0.02	58.00 ± 10.13
tap14	5	9/10/20 9:02	0.25 ± 0.04	70.00 ± 10.13
tap15	4	9/10/20 9:21	0.11 ± 0.04	25.26 ± 10.13
tap18	5	9/22/20 9:10	0.27 ± 0.03	79.68 ± 10.13
tap19	4	9/22/20 9:26	0.20 ± 0.02	49.58 ± 10.13
tap20	5	10/1/20 8:10	0.27 ± 0.02	79.40 ± 10.13

tap21	4	10/1/20 8:25	0.14 ± 0.02	32.71 ± 10.13
tap26	4	10/22/20 8:35	0.19 ± 0.02	49.13 ± 10.13
tap30	4	10/29/20 8:50	0.15 ± 0.02	36.50 ± 10.13
tap32	5	11/12/20 8:35	0.31 ± 0.04	96.64 ± 10.13
tap35	4	11/19/20 8:35	0.16 ± 0.30	39.3 ± 10.13

The water age at station 4 was 48.21 ± 25.30 hours (n = 6, ± 1 SD) and the water age at station 5 was 76.74 ± 14.21 hours (n = 5, ±1 SD). As hypothesized, the water age increased distally from the plant (fig. 22). Water age also increased seasonally, suggesting decreasing water usage during the cooler months; most likely because of a reduction in sprinkler usage (North Shore Water Commission 2020).

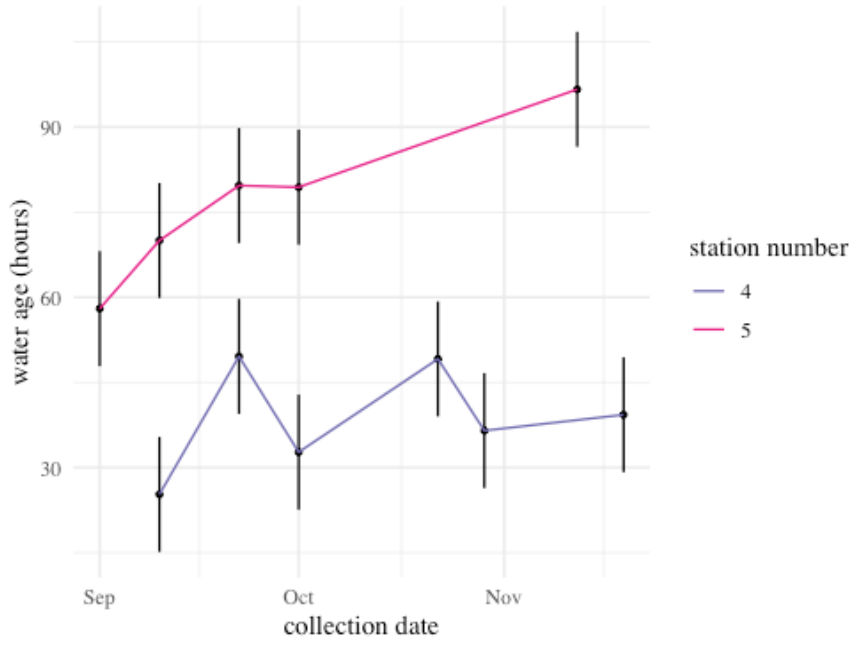

Figure 22: Resolved water ages for stations 4 & 5.

On the three sampling dates wherein water ages from both stations 4 & 5 were resolved, the water age increased by 40.5 ± 9.1 hours (n = 3, ±1 SD) from station 4 to station 5. The low standard deviation may indicate that water usage between stations 4 and 5 is relatively stable, resulting in similar water age

intervals; however, more samples would be necessary to draw robust conclusions. The water age did not appear to correlate strongly to any water chemistry parameter (fig. 23). Water chemistry parameters at stations 4 and 5 were more similar to each other on any particular day than the chemical parameters were at any single station between sampling dates, suggesting that water chemistry changed little over the observed ~40 hour difference in retention time between the two stations.

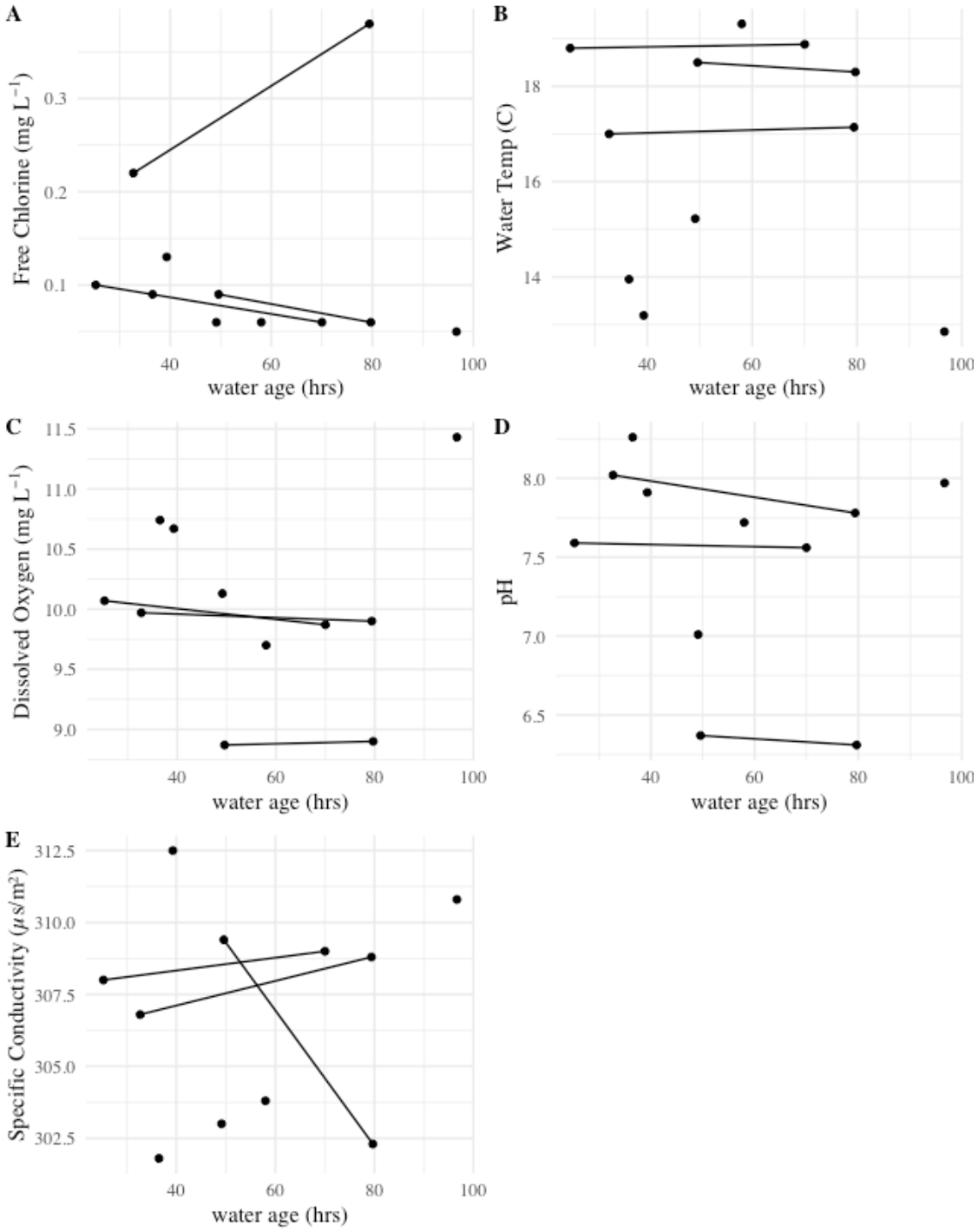

Figure 23: Water age plotted against free chlorine (A), water temperature (B), dissolved oxygen (C), pH (D), and specific conductivity (E). Samples collected on the same date are connected by a line, which does not indicate continuously measured data. delineated.

One instance of free chlorine rising with water age occurred on 10/1/2020, several days after an issue occurred in the treatment plant which caused high levels of disinfectant to enter the flowing water. The

exact time at which the issue began is not known; however, evidently, the water collected at the most distal station originated from the plant while the issue was still occurring, about 3 days prior to sampling. On the other two dates on which samples at both stations 4 and 5 were collected, the chlorine residual declined with water age at a similar rate, 8.94E-4 mg L^{-1} chlorine/hour on 9/10/20 and 9.97E-4 mg L^{-1} chlorine/hour on 9/22/20. Because the Hach kit used to measure chlorine has a precision of ± .01 mg L^{-1} chlorine, calculating water age from the chlorine residual is not practicable. The water age estimates were next compared to the microbial data, and the results are discussed in in chapter 4.

To refine the water aging technique for future studies, and to better understand the high ^{90}Y activities measured close to the treatment plant, a final experiment was conducted.

Introduction, Particulate Experiment:

To determine if particle fractionation of ^{90}Y occurs in the pipe system, the following samples were taken from station 1 on 04/28/21:

Table 8: Description of particulate experiment samples.

Sample Type	Description	N Samples Incubated	N Samples Unincubated
Particulate Fraction (PF)	The water from the hydrant was filtered on to a 0.45 µm filter prior to any addition of iron or acid. The filter was then dissolved in HNO_3 and processed separately from the dissolved fraction according to the protocol described below.	2	0
Dissolved Fraction (DF)	Water from the hydrant was filtered on to a 0.45 µm filter. Iron and HCl were added to the eluent and the sample was processed according to the ^{90}Y counting protocol described above.	1	1

Whole Fraction (WF)	Samples were processed according to the ^{90}Y counting protocol described above.	1	1

The ^{90}Y activity in the DF was compared to the ^{90}Y activity in the PF to determine the extent to which ^{90}Y associated with particles. The incubated WF and DF were measured for ^{90}Sr to determine the starting concentration of ^{90}Sr at station 1.

Methods, Particulate Experiment, Particle Fraction (PF):

For the PF, collected on a 0.45 µm pre-filter, the filters were incubated for two weeks to allow ^{90}Y to grow into equilibrium with ^{90}Sr. The filters were then placed in a large beaker, and 2 ml of ^{88}Y were added as a yield monitor. Then, 20 ml of concentrated nitric acid were poured over the filter. The beaker was covered with a watch glass, placed on a hot plate, and simmered for approximately two hours. Then, while maintaining low heat, the watch plate was removed, allowing the nitric acid to evaporate. Heat was maintained until the sample formed a crust on the surface of the beaker, after about one hour. Next the crust was dissolved in 30 ml of 0.1M HCl. The 30 ml was eluted through a prepared anion column. Two mg of ferrous iron (added as a ferrous sulfate solution) was pipetted into the eluent, and concentrated ammonium hydroxide was titrated into the eluent until its pH rose to about ten. The eluent was then filtered onto a nitrocellulose filter (.45 um, 17 mm, Millipore) and the counting process was completed as above.

Results, Particulate Experiment:

Unfortunately, a procedural error in the processing of the particulate fractions resulted in those samples being lost. The ^{90}Y eluted from the anion column did not bind to the ferrous sulfate solution. The results of the samples for which ^{90}Y was measured are displayed below (table 9).

Table 9: Results from the incubation experiment

Sample Type	^{90}Y Activity ± error (dpm L^{-1})
WF, unincubated	0.48 ± 0.06
PF, unincubated	ND

DF, unincubated	0.00 ± 0.02
WF, incubated 2 weeks	0.60 ± 0.05
PF, unincubated	ND
DF, incubated 2 weeks	0.45 ± 0.04

Like the samples collected at station 1 during the field campaign in the fall and winter of 2020, these samples contain high activities of ^{90}Y. The ^{90}Y activity of the unincubated WF (whole fraction) was 0.48 ± 0.06 dpm L^{-1}, which is equivalent to the ^{90}Sr activity determined in the incubation experiment at SFS (0.47 ± 0.4 dpm L^{-1}, n = 6, ± 1 SD). The ^{90}Y activity in the DF (dissolved fraction) sample, however, was below detection (~0 dpm L^{-1}), corroborating our earlier hypothesis that high levels of ^{90}Y activity must have been on particulate matter. Indeed, photographs of the column separation procedure showed significant particulate material associated with the unfiltered sample (fig. 24)

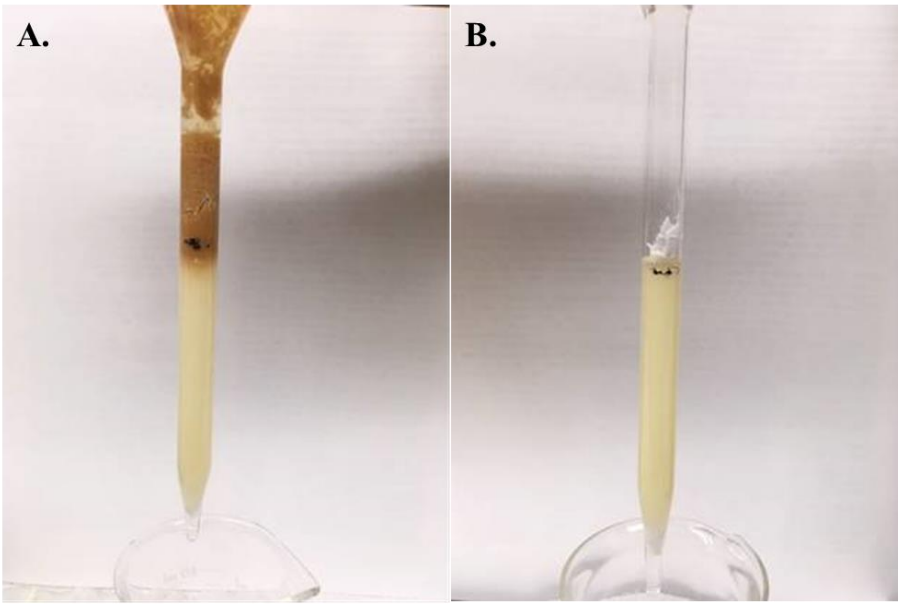

Figure 24: The filtrate of the WF (A) and the PF (B) of the particulate experiment.

^{90}Y activity in the incubated DF sample was 0.45 ± 0.04 dpm L^{-1}, which again showed that the dissolved ^{90}Sr activity in the NSWC distribution was equal to what was found in SFS tap water. ^{90}Y activity in the incubated WF sample was slightly higher at 0.60 ± 0.05 dpm L^{-1}; however, with only one sample (n = 1), we cannot say with any certainty that a higher activity of

^{90}Sr was observed (in the form of e.g., a strontium carbonate precipitate). A more likely explanation for the high ^{90}Y activities that were observed at station 1 (i.e., 3.1 dpm L^{-1} on 11/12/202) and – to a lesser extent – at station 3 is that sedimented particulate matter containing ^{90}Y was resuspended in the pipe network when the hydrants were flushed before sampling. Although ^{90}Y activity cannot exceed the ^{90}Sr activity in a closed system, the distribution network is an open system, and regional inventories of ^{90}Y/^{90}Sr activity ratios > 1 are possible. Although we do not believe that the scavenging of ^{90}Y from the water stream to the pipe/deposit surface is significant (< 5%), resuspended activities of ^{90}Y can severely impact estimates of local water age. Additional tests on how tap water can be collected without disturbing the sedimented deposit load are required. In the following chapter, the microbial community is compared with the resolved water ages to analyze the temporal trends in the data.

CHAPTER 4 – THE EFFECT OF WATER AGE ON THE MICROBIOLOGICAL COMMUNITY

Introduction:

Because there are so little nutrients in tap water, the bacterial community is especially sensitive to small changes in chemical parameters such as temperature, pH, dissolved oxygen, and nutrient loads (El-Chakhtoura et al. 2018). In such oligotrophic environments, the composition and concentration of nutrients play a pronounced role in shaping the microbial community. Disinfectant residual has been found to be especially important in shaping drinking water communities; for example, LeChavallier et al (1996) found that as disinfectant residuals decreased below 0.2 mg/L for chlorine or 0.5 mg/l for chloramine, the concentration of coliform bacteria increased significantly (Lechevallier, Welch, and Smith 1996).

In a similar study, Wang et al. (2012), tested water slowly moving through a lab-scale system of pipes to simulate aging water. Using principal component analyses (PCA), their data showed that bacterial communities separated according to water age, with dissolved oxygen and disinfectant residual driving the overall trend (Wang et al. 2012). Because the sequencing data was influenced by low DNA concentrations, and therefore did not have an identifiable distribution, a non-metric multidimensional scaling analysis (NMDS) was used to explore the relationship of the community composition to the field parameters: NMDS, unlike PCA, are robust to data which do not have an identifiable distribution.

An NMDS is a statistical method designed to compress many dimensions into two dimensions for ease of visual interpretation. The BCD was used to compress the community composition data in this NMDS. As explained in chapter 2, the BCD is a pair-wise distance measurement which approximates the dissimilarity between the compositions of two samples. An NMDS model iterates over *n* permutations to arrange all the pairwise distance scores on to two-dimensional space. The user defines, k, which is the starting number of dimensions over which the algorithm attempts to place the data points. Once the model converges on an arrangement of points that best preserves all the BCD values between each pair of samples, the iterative modelling process ends. The end-result of the NMDS is a two-dimensional plot of each

sample, with arbitrary axes. Visually, samples that cluster together share similar community compositions.

To determine the extent to which dissolved oxygen, free chlorine, pH, and water temperature drove community separation, an environmental fitting function was performed on the NMDS ordination using the *envfit* function in the package, *vegan* (RB et al. 2013). For each continuous variable, the *envfit* function fits a linear trend surface through the NMDS points in the n-dimensional ordination space. Visually, the function is plotted on the two-dimensional plot as an arrow pointing in the direction of the steepest gradient of the plane in the n-dimensional space, i.e., the arrow points in the direction in which the environmental variable was most related to the distance between samples.

On the NMDS ordination, samples that clustered spatially were analyzed using the r package, *indicator species* (De C´aceres 2020). The function assigns an indicator value to measure the association between a species and a group of samples, e.g., a site from which the species were sampled. Like the NMDS, the *indicator species* function is permutational: the samples are randomly subsampled n-times, and the frequency that a certain species is present in a subsample from one site, and not another determines its indicator value. The results of the indicator species test help to show which species are most tightly associated with each group of samples.

Because the water age of only 12 samples was resolved, a separate NMDS model was created to show community change in response to water age in those samples. The 12 resolved water-ages were binned into three groups: ages below the second quantile (25 – 39 hours) were "young," ages between the second and third quantile (49 – 58 hours) were "moderate," and ages at or above the fourth quantile (79 – 97 hours) were "old." An NMDS was then run on the 12 microbial samples with resolved water age measurements to determine if microbial communities clustered by the three age groups. An indicator species analysis was performed to determine which taxa were most likely to be associated with each water age class. Finally, to determine whether broad-scale community level differences correlate to water age, the community data was binned according to lake, pipe, and potentially pathogenic microbes: The binned community data were then compared to the binned water age data.

Methods:

Computation for the NMDS analyses was conducted in R, using the vegan package and the function, *metaMDS* therein (RB et al. 2013). The distance matrices were computed using the bray function, and the modelling engine was set to monoMDS. After creating the model, the function *envfit* was called to model dissolved oxygen, water temperature, and free chlorine as a function of community relatedness. The results from the *envfit* model were then displayed on the two dimensional NMDS ordination space as arrows pointing in the direction of strongest correlation.

For the coarse-grained water age analysis, the following bins were used to categorize the microbial taxonomy data: lake-origin microbes, pipe-wall associated microbes, and pathogenic microbes. Pipe and lake ASVs were identified by comparing the drinking water 16S rRNA ASVs to a database of iron pipe scale 16S rRNA ASVs, and Lake Michigan 16S rRNA ASVs (Kimbell et al. 2021; Newton et al. 2011). Drinking water ASVs that were 100% identical to ASVs in each respective database were binned accordingly. Organisms classified as pathogenic (at the genus taxonomic level) by the EPA guidance document on drinking water microbial growth were binned as pathogens (EPA 2002).

Results & Discussion:

NMDS, All Samples:

The NMDS of the 32 samples was constructed with a starting dimension of $k = 10$. The stress of the resulting model was, 0.03, indicating that the model fit the data strongly. Visual inspection of the NMDS revealed a clear seasonal pattern in community composition (fig. 25).

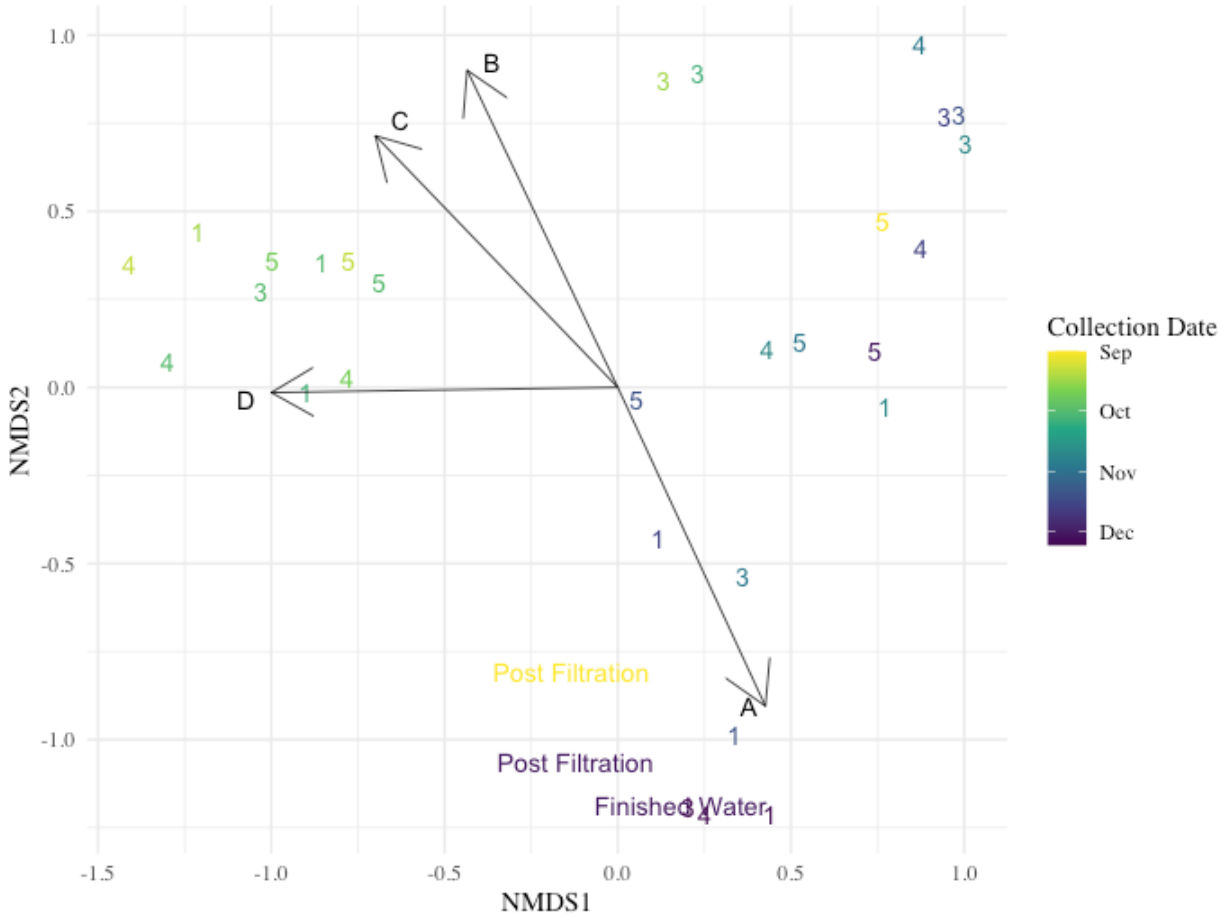

Figure 25: NMDS results of all samples labelled by station number, color-coded by sample collection date. The environmental fitting function results are displayed as arrows originating at the origin and pointing towards the direction of strongest correlation to sample separation. Arrows A is DO, B is water temperature, C is free chlorine, and D is pH.

The samples cluster into three groups, an early season group, a late season group, and a group found in the treatment plant. The influence of DO, water temperature, and free chlorine on sample separation were all significant ($p < 0.05$). Water temperature and DO tended to have the opposite effect on community differences: as temperature and DO are inversely related. Higher pH tended to pull the samples into the early season group, suggesting that pH is an important seasonal parameter. Because the field samples approximately clustered into a September – Mid-October group, and a Mid-October – December group, and the samples from the treatment plant formed a cluster, an indicator species analysis was performed to determine which taxa were most closely associated with each group. The taxa associated most strongly with the early season group were members of the family, *Gallionellaceae* which are commonly found growing on pipe

walls (Kimbell et al. 2021, Emerson 2018). This may be indicative of increased corrosion in the summer months as a result of higher water temperatures which increase the rate of iron oxidation (McNeill and Edwards 2002). The taxa most strongly associated with the treatment plant were of the phylum, *Firmicutes. Firmicutes* form a small percentage of Lake Michigan biome, but are often found in treatment plant biofilms (Newton et al. 2011; Luo et al. 2013). No taxa were significantly associated with the Mid-October through December group.

NMDS, Samples With Water Age:

A second NMDS was run on the subset of samples with resolved water age measurements (n = 11) (fig. 26). The water age was only resolved for stations 4 & 5 because of high ^{90}Y readings measured at stations 1 & 3, which indicated the influence of a reservoir of ^{90}Y with an unknown, potentially variable activity. On the NMDS, the starting number of dimensions was set to, $k = 3$, and the stress of the resulting model was 0.078, indicating that the model fit the data moderately strong.

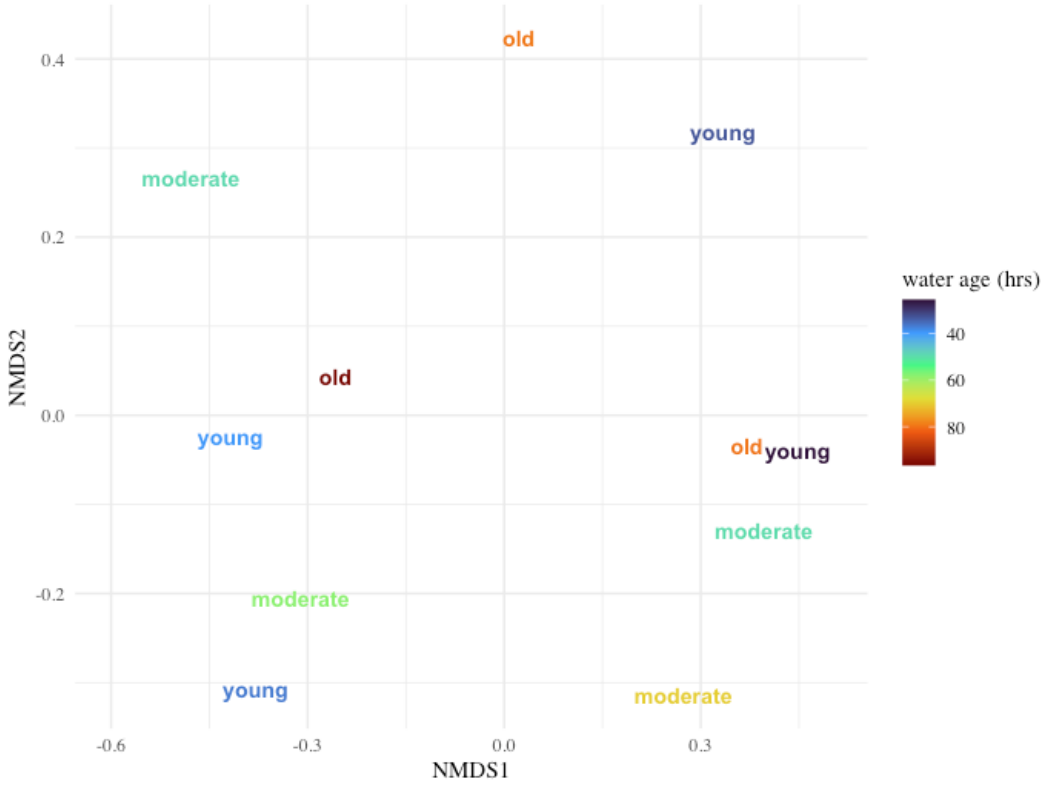

Figure 26: NMDS results of all samples labelled by water age classification, color-coded by radionuclide-derived water age.

The water age does not appear to be a driver of community change in the range of water ages sampled (25 – 97 hours). Previous studies have shown that alpha diversity of microbial communities does not change significantly until sampling points are separated by long distances (> 46 km); hence, it is possible that only water ages higher than those studied significantly influence microbial community composition (A. Pinto et al. 2014). As shown in chapter 2, most of the microbial community in any one sample was common to other samples; therefore, any changes that did occur in the microbial communities may simply be indicative of stochastic processes such as biofilm sloughing.

An indicator species analysis was performed to determine which microbes were most closely associated to each age class of water. In young water (25 – 39 hours) two members of the *Gammaproteobacteria,* and one member of the order *Bacilli* were found to be positively indicators. These taxa commonly form spores, and therefore, may have survived the treatment plant process and remained in the flowing water. An unidentified member of the phylum, *Firmicutes* was significantly associated with moderately aged water (49 – 58 hours). Members of *Firmicutes* are often inhabitants of biofilms, which, may suggest that between 49 and 60 hours flowing water begins to accumulate organisms from the biofilm. No microbes were significantly associated with old water (79 – 97 hours).

Pipe, Lake, Pathogen, Water Age Analysis

To determine if a coarser grained resolution would reveal patterns in the water age data, rather than using all the taxonomic information, the OTUs were binned into either lake, pipe, or pathogen associated groups. The most common lake phyla present in the drinking water microbial communities were the phyla, *Proteobacteria, Actinobacteria, Bacteriodeta, Nitrospirota, Cyanobacteria, Planctomycetota, Verrumicrobia, Deinococcota,* and *Bdellovibrionota*. Within the phylum *Proteobacteria,* members of the classes *Alphaproteobacteria* , and *Gammaproteobacteria* were the most the common organisms positively identified. *Alphaproteobacteria* are common heterotrophic endosymbionts and intracellular parasites, and *Gammaproteobacteria* originate in the digestive systems of animals, but persist at low concentrations in natural freshwater environments. Organisms within the genus *Nitrospira* were the only nitrifiers positively identified in this study. Many of the *Cyanobacteria*

identified were associated with the chloroplast genome, and not the organismal genome target by the 16S primers; consequently these ASVs were not considered in further analyses.

Phyla identified in the pipe wall subgroup of organisms were mostly shared with the lake group, except for the *Firmicutes, Campilobacterota, Acidobacteria,* and *Patescibacteria* (Kimbell et al. 2021). All of stations investigated in this study were situated above sections of the water main composed of cast iron. The free iron in the flowing water, likely contributed to the growth of iron oxidizers such as *Gallionella.* and the *Sphaerotilus-Leptothrix* group (SLG) These organisms are commonly associated with water system biofilms (Schmidt et al. 2014). Other chemoautotrophs commonly found on pipe walls, such as, the sulfate-metabolizing genera, *Desulfosporosinus,* and *Sulfuricurvum,* were identified. Although several instances of high ^{90}Y activity occurred at station 1, indicating that a high degree of biofilm sloughing may have been occurring, an *indicSpecies* analysis did not identify any organisms significantly associated exclusively with station 1.

The pathogens identified in this study include, *Yersinia enterocolitica, Legionella pneumophila, Flavobacterium* spp., and *Pseudomonas*. *Yersinia* are motile with peritrichous flagella when grown below 30°C: They use nitrate as their oxidizing agent. The species, *Yersinia enterocolitica* is known to cause gastroenteritis. *Legionella*, do not form spores, are unencapsulated, aerobic, and require iron salts for growth. They are often found associated with free-living environmental amoeba in aquatic environments. They are pathogenic in humans and are the cause of the lung disease, Legionnaire's disease (Brenner, Krieg, and Staley 2005). *Flavobacterium* are obligate aerobes and about half the species can reduce nitrate to nitrite. They are sometimes found multiplying in diseased fish (Ludwig, Euzéby, and Whitman 2010). *Psuedomonas* encompass a diverse group of species, most are aerobes and produce biofilms. One of the most common environmental species of the *pseudomonads, P. aeruginosa,* is often implicated in hospital-acquired infections (Hassett et al. 2002). The organism can cause corneal infections and may complicate respiratory ailments (Garrity 2007).

After binning each of the OTUs, the total lake, pipe, and pathogen OTUs in each sample were computed. Then, the binned counts were divided by the total counts in each sample to determine the relative group abundances per sample. The relative abundances of each of the

three groups were then compared to the binned water ages to observe coarse-grain change in the community structure (fig. 27).

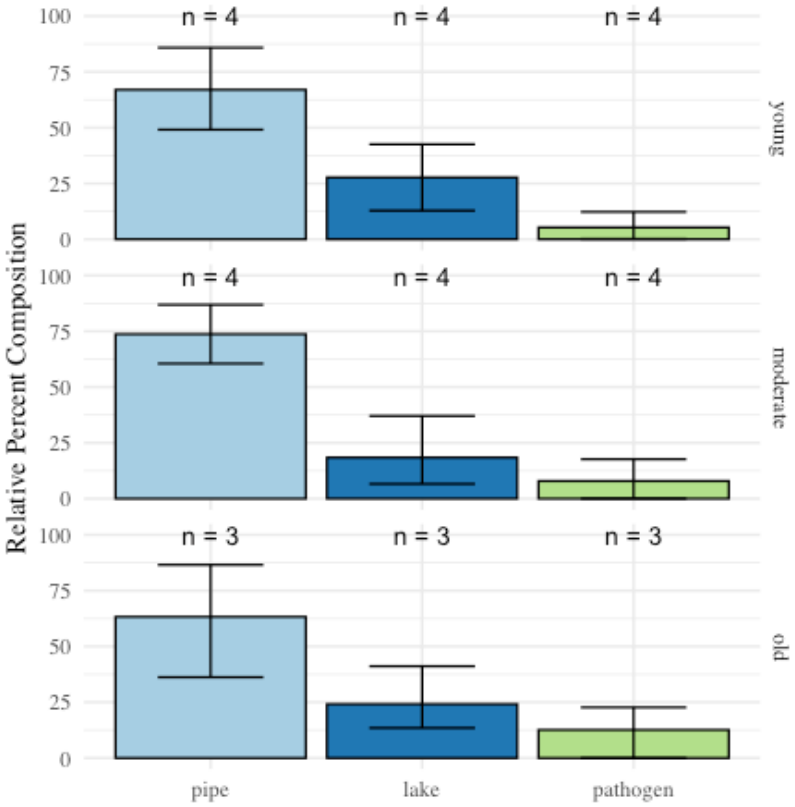

Figure 27: Barplot of the mean relative compositions of pipe, lake, and pathogen microbes found in stations 4 & 5, arranged by young (25 – 39 hours), moderate (49 – 58 hours), and old (79 – 97 hours) water ages. The error bars are the upper and lower Gaussian confidence limits based on the t-distribution.

The pipe OTUs dominated across all three classes of water ages, indicating that OTUs originating from the pipe wall composed most of the bulk water composition. The results of an ANOVA test suggest that the mean pipe OTU relative composition did not change significantly across water age groups ($f_{2,8} = 0.22$, $p = 0.88$). The lake OTUs were the second most common group across all three water age classes. Because the DNA isolation process does not distinguish between live and dead cells, these organisms may have survived the water treatment process, or they may be inactivated. According to an ANOVA, the mean lake OTU relative composition did not change significantly as water aged from 25 to 97 hours ($f_{2,8} = 0.29$, $p = 0.76$), indicating that lake microbe regrowth was likely not occurring, and that the lake organisms detected may have been deactivated. The pathogen group composed the lowest percentage of the binned data.

Although the mean pathogen relative abundance increased from 5.3 ± 7.6% (mean ± 1 sd) in young water (25 – 39 hours) to 12.6 ± 11.5% in old water (79 – 97 hours), an ANOVA did not suggest any significant differences amongst the three water age groups ($f_{2,8} = 0.46$, $p = 0.65$). In one old sample (79 – 97 hours), a single high reading (13.9%) of *flavobacterium sp.* contributed most to the high mean pathogenic water age.

CHAPTER 5 – CONCLUSION AND FUTURE DIRECTIONS

At the spatial scale studied (0 - 5.8 km from the treatment plant), the microbial community correlates weakly with water age. Following water treatment, a community of lake microbes remained in the pipe system. The flowing water was then seeded by the pipe biofilm near the treatment plant, and a core group of microbes was established. Past studies have observed a similar trend: Researchers have hypothesized that the bulk water is seeded by microbes close to the treatment plant, and that this community determines the core microbiome (A. Pinto et al. 2014). Furthermore, many studies have found a consistent core community that is relatively constant throughout distribution systems (El-Chakhtoura et al. 2015; Potgieter et al. 2018). After becoming established, the core community has been shown to remain stable until sampling points are separated by > 46 km (A. Pinto et al. 2014). Water age at any particular site tended to vary more than expected, ranging from 25.3 – 49.58 hours at station 4, and 58.0 – 96.6 hours at station 5, indicating that water age is loosely correlated to pipe distance. A seasonal increase in water age, likely associated with decreased lawn maintenance, was also observed.

Evidently, a reservoir of unsupported ^{90}Y exists in the pipe system near the treatment plant. The reservoir is likely bound to the pipe scale, sloughing at stochastic rates. To minimize the likelihood of sloughing, future studies should either flush the hydrants for long periods of time (> 10 minutes), or sample domestic taps. Long flushing times will not substantially alter the location from which water was sampled because the volume of flushed water is significantly lower than the volume of water within the pipe system.

Even after combining the filtrate from two 3-liter samples, the extracted DNA concentrations were low and contributed to poor precision in the microbial data. In the future, when samples are collected from hydrants, pre-filters should be used to remove particulates resuspended by high water pressure. Specifically, a serial filtration set-up, in which water is filtered at 0.5 µm, and then at 0.22 µm is recommended. The 0.5 µm filter should be replaced several times to ensure that at least 10 liters of water have passed through the 0.22 µm. DNA from the larger filter could be analyzed to determine which microbes are particle associated, and, similarly, the smaller filter could be analyzed separately to determine which microbes are planktonic.

The results of this thesis have helped to elucidate the planktonic community dynamics in the Whitefish Bay distribution system. The system appeared to be dominated by seasonal influences, more so than by pipe distance, indicating that the water in this system is highly stable. Another positive outcome of this research was the refining of the $^{90}Sr/^{90}Y$ water aging protocol. In the past, Waples (2015) employed a method wherein the particle fraction of ^{90}Y was isolated separately from the dissolved fraction of ^{90}Y (Waples et al. 2015). The two fractions of ^{90}Y were then combined and counted simultaneously. In this study, the two fractions of ^{90}Y were isolated in one step, thereby reducing the sample processing time by approximately 6 hours. The corroboration of the data collected by this abridged methodology (see *Results, Time Series Experiment*) represents a substantial gain in water-age sample processing efficiency.

Overall, the results of this thesis, although not conclusive, offer solid footing on which to design future experiments. In particular, future research should measure the extent to which the measured ^{90}Y activity in flowing water originated from the reservoir of ^{90}Y associated to the pipe wall. To this end, I recommend performing multiple time series experiments from water collected from one location at one time. For each time series, I would filter the water at a different pore size. Then, I would analyze each time series to determine which pore size filter yielded the most accurate water age estimate, and which filter sizes tended to over-estimate the water age. Similarly, for any future DNA work conducted in iron-rich drinking water, I would recommend filtering at multiple pore sizes and comparing both the yield of DNA and the microbial composition of each pore size.

REFERENCES

Allen, Martin J, Stephen C Edberg, and Donald J Reasoner. 2004. “Heterotrophic Plate Count Bacteria—What Is Their Significance in Drinking Water?” *International Journal of Food Microbiology* 92: 265–74. https://doi.org/10.1016/j.ijfoodmicro.2003.08.017.

Baldani, José Ivo, Luc Rouws, Leonardo Magalhães Cruz, Fábio Lopes Olivares, Michael Schmid, and Anton Hartmann. 2014. “The Family Oxalobacteraceae BT - The Prokaryotes: Alphaproteobacteria and Betaproteobacteria.” In , edited by Eugene Rosenberg, Edward F DeLong, Stephen Lory, Erko Stackebrandt, and Fabiano Thompson, 919–74. Berlin, Heidelberg: Springer Berlin Heidelberg. https://doi.org/10.1007/978-3-642-30197-1_291.

Bitton, Gabriel. 2014. “Microbiological Aspects of Drinking Water Treatment.” *Microbiology of Drinking Water*, 29–64. https://doi.org/10.1002/9781118743942.ch2.

Brenner, Don J, Noel R Krieg, and James T Staley. 2005. *Bergey’s Manual® of Systematic Bacteriology: Volume Two The Proteobacteria Part C The Alpha-, Beta-, Delta-, and Epsilonproteobacteria*. Springer.

Brenner, Don J, Noel R Krieg, James T Staley, and George M Garrity. 2005. *Bergey’s Manual® of Systematic Bacteriology: Volume Two: The Proteobacteria, Part A Introductory Essays*. Springer.

Butler, John M, and Carolyn R Hill. 2010. “Scientific Issues with Analysis of Low Amounts of DNA.” *Promega Website*, 1–8.

C´aceres, Miquel De. 2020. “How to Use the Indicspecies Package (Ver. 1.7.8).”

Callahan, Benjamin J, Paul J McMurdie, Michael J Rosen, Andrew W Han, Amy Jo A Johnson, and Susan P Holmes. 2016. “{DADA2}: High-Resolution Sample Inference from Illumina Amplicon Data.” *Nat. Methods* 13 (7): 581–83. https://doi.org/10.1038/nmeth.3869.

Chan, Sandy, Kristjan Pullerits, Alexander Keucken, Kenneth M. Persson, Catherine J. Paul, and Peter Rådström. 2019. “Bacterial Release from Pipe Biofilm in a Full-Scale Drinking Water Distribution System.” *Npj Biofilms and Microbiomes* 5 (1): 3–10. https://doi.org/10.1038/s41522-019-0082-9.

Characklis, Gregory W, Mackenzie J Dilts, Otto D Simmons, Christina A Likirdopulos, Leigh-Anne H Krometis, and Mark D Sobsey. 2005. “Microbial Partitioning to Settleable Particles in Stormwater.” *Water Research* 39 (9): 1773–82. https://doi.org/https://doi.org/10.1016/j.watres.2005.03.004.

Chlorine Chemistry Council. 2003. “Drinking Water Chlorination.”

Davis, Nicole M, Diana M Proctor, Susan P Holmes, David A Relman, and Benjamin J Callahan. 2017. “Simple Statistical Identification and Removal of Contaminant Sequences in Marker-Gene and Metagenomics Data.” https://doi.org/10.1101/221499.

El-Chakhtoura, Joline, Emmanuelle Prest, Pascal Saikaly, Mark van Loosdrecht, Frederik Hammes, and Hans Vrouwenvelder. 2015. “Dynamics of Bacterial Communities before and after Distribution in a Full-Scale Drinking Water Network.” *Water Research* 74 (0): 180–90. https://doi.org/10.1016/j.watres.2015.02.015.

El-Chakhtoura, Joline, Pascal E. Saikaly, Mark C.M. Van Loosdrecht, and Johannes S. Vrouwenvelder. 2018. “Impact of Distribution and Network Flushing on the Drinking Water Microbiome.” *Frontiers in Microbiology* 9 (SEP): 1–13. https://doi.org/10.3389/fmicb.2018.02205.

Emerson, David. 2018. “The Role of Iron-Oxidizing Bacteria in Biocorrosion: A Review.” *Biofouling* 34 (9): 989–1000.

England, Matthew H., and Ernst Maier-Reimer. 2001. “Using Chemical Tracers to Assess Ocean Models.” *Reviews of Geophysics* 39 (1): 29–70. https://doi.org/10.1029/1998RG000043.

EPA. 1989. “Surface Water Treatment Rules.” Drinking Water Requirements for States and Public Water Systems. 1989. https://www.epa.gov/dwreginfo/surface-water-treatment-rules.

———. 2002. “Health Risks from Microbial Growth and Biofilms in Drinking Water Distribution Systems.” *EPA Office of Groundwater and Drinking Water*. Washington DC. https://doi.org/10.1017/CBO9781107415324.004.

———. 2018. “2018 Edition of the Drinking Water Standards and Health Advisories Tables,” no. March.

Feely, Herbert, W., Herbert L. Volchok, Edward P. Hardy Jr., and Lawrence E. Toonkel. 1978. "Worldwide Deposition of Strontium-90 through 1976." *Evironmental Science and Technology* 12 (7): 808–9.

Garner, Emily, Jean McLain, Jolene Bowers, David M. Engelthaler, Marc A. Edwards, and Amy Pruden. 2018. "Microbial Ecology and Water Chemistry Impact Regrowth of Opportunistic Pathogens in Full-Scale Reclaimed Water Distribution Systems." Research-article. *Environmental Science and Technology* 52 (16): 9056–68. https://doi.org/10.1021/acs.est.8b02818.

Garrity, George. 2007. *Bergey's Manual® of Systematic Bacteriology: Volume 2: The Proteobacteria, Part B: The Gammaproteobacteria*. Vol. 2. Springer Science & Business Media.

Goodrich, Julia K., Sara C. Di Rienzi, Angela C. Poole, Omry Koren, William A. Walters, J. Gregory Caporaso, Rob Knight, and Ruth E. Ley. 2014. "Conducting a Microbiome Study." *Cell* 158 (2): 250–62. https://doi.org/10.1016/j.cell.2014.06.037.

Hallbeck, Lotta, and Karsten Pedersen. 2014. "The Family Gallionellaceae BT - The Prokaryotes: Alphaproteobacteria and Betaproteobacteria." In , edited by Eugene Rosenberg, Edward F DeLong, Stephen Lory, Erko Stackebrandt, and Fabiano Thompson, 853–58. Berlin, Heidelberg: Springer Berlin Heidelberg. https://doi.org/10.1007/978-3-642-30197-1_398.

Hassett, Daniel J, John Cuppoletti, Bruce Trapnell, Sergei V Lymar, John J Rowe, Sang Sun Yoon, George M Hilliard, Kislay Parvatiyar, Moneesha C Kamani, and Daniel J Wozniak. 2002. "Anaerobic Metabolism and Quorum Sensing by Pseudomonas Aeruginosa Biofilms in Chronically Infected Cystic Fibrosis Airways: Rethinking Antibiotic Treatment Strategies and Drug Targets." *Advanced Drug Delivery Reviews* 54 (11): 1425–43.

Joshi, S.R. 1991. "Radioactivity in the Great Lakes." *Science of the Total Environment2* 100: 61–104.

Jumas-Bilak, Estelle, Laurent Roudière, and Hélène Marchandin. 2009. "Despcription of 'Synergistetes' Phyl. Nov. and Emended Description of the Phylum 'Deferribacteres' and of

the Family Syntrophomonadaceae, Phylum 'Firmicutes.'" *International Journal of Systematic and Evolutionary Microbiology* 59 (5): 1028–35. https://doi.org/10.1099/ijs.0.006718-0.

Kielak, Anna M., Cristine C. Barreto, George A. Kowalchuk, Johannes A. van Veen, and Eiko E. Kuramae. 2016. "The Ecology of Acidobacteria: Moving beyond Genes and Genomes." *Frontiers in Microbiology* 7 (MAY): 1–16. https://doi.org/10.3389/fmicb.2016.00744.

Kimbell, Lee K., Emily Lou Lamartina, Anthony D. Kappell, Jingwan Huo, Yin Wang, Ryan J. Newton, and Patrick J. McNamara. 2021. "Cast Iron Drinking Water Pipe Biofilms Support Diverse Microbial Communities Containing Antibiotic Resistance Genes, Metal Resistance Genes, and Class 1 Integrons." *Environmental Science: Water Research and Technology* 7 (3): 584–98. https://doi.org/10.1039/d0ew01059f.

Knight, Rob, Alison Vrbanac, Bryn C. Taylor, Alexander Aksenov, Chris Callewaert, Justine Debelius, Antonio Gonzalez, et al. 2018. "Best Practices for Analysing Microbiomes." *Nature Reviews Microbiology* 16 (7): 410–22. https://doi.org/10.1038/s41579-018-0029-9.

Koops, H-P, B Böttcher, U C Möller, a Pommerening-Röser, and G Stehr. 1991. "Classification of Eight New Species of Ammonia-Oxidizing Bacteria." *Journal of General Microbiology* 137 (7): 1689–99. http://mic.sgmjournals.org/cgi/doi/10.1099/00221287-137-7-1689.

Lautenschlager, Karin, Chiachi Hwang, Fangqiong Ling, Wen Tso Liu, Nico Boon, Oliver Köster, Thomas Egli, and Frederik Hammes. 2014. "Abundance and Composition of Indigenous Bacterial Communities in a Multi-Step Biofiltration-Based Drinking Water Treatment Plant." *Water Research* 62: 40–52. https://doi.org/10.1016/j.watres.2014.05.035.

Lautenschlager, Karin, Chiachi Hwang, Wen Tso Liu, Nico Boon, Oliver Köster, Hans Vrouwenvelder, Thomas Egli, and Frederik Hammes. 2013. "A Microbiology-Based Multi-Parametric Approach towards Assessing Biological Stability in Drinking Water Distribution Networks." *Water Research* 47 (9): 3015–25. https://doi.org/10.1016/j.watres.2013.03.002.

Lechevallier, Mark W., Nancy J. Welch, and Darrell B. Smith. 1996. "Full-Scale Studies of Factors Related to Coliform Regrowth in Drinking Water." *Applied and Environmental Microbiology* 62 (7): 2201–11. https://doi.org/10.1128/aem.62.7.2201-2211.1996.

Lee, Jung, Harshit Mahandra, Guillermo Alvial Hein, Juliana Ramsay, and Ahmad Ghahreman. 2021. “Toward Sustainable Solution for Biooxidation of Waste and Refractory Materials Using Neutrophilic and Alkaliphilic Microorganisms—A Review.” *ACS Applied Bio Materials* 4 (3): 2274–92.

Li, Qing-Mei, Ying-Li Zhou, Zhan-Fei Wei, and Yong Wang. 2021. “Phylogenomic Insights into Distribution and Adaptation of Bdellovibrionota in Marine Waters.” *Microorganisms* . https://doi.org/10.3390/microorganisms9040757.

Li, Weiying, Junpeng Zhang, Feng Wang, Lin Qian, Yanyan Zhou, Wanqi Qi, and Jiping Chen. 2018. “Effect of Disinfectant Residual on the Interaction between Bacterial Growth and Assimilable Organic Carbon in a Drinking Water Distribution System.” *Chemosphere*. https://doi.org/10.1016/j.chemosphere.2018.03.056.

Lienard, J., A. Croxatto, A. Gervaix, Y. Lévi, J. F. Loret, K. M. Posfay-Barbe, and G. Greub. 2017. “Prevalence and Diversity of Chlamydiales and Other Amoeba-Resisting Bacteria in Domestic Drinking Water Systems.” *New Microbes and New Infections* 15: 107–16. https://doi.org/10.1016/j.nmni.2016.10.003.

Lu, J., I. Struewing, S. Yelton, and N. Ashbolt. 2015. “Molecular Survey of Occurrence and Quantity of Legionella Spp., Mycobacterium Spp., Pseudomonas Aeruginosa and Amoeba Hosts in Municipal Drinking Water Storage Tank Sediments.” *Journal of Applied Microbiology* 119 (1): 278–88. https://doi.org/10.1111/jam.12831.

Ludwig, Wolfgang, Jean Euzéby, and William B. Whitman. 2010. “Road Map of the Phyla Bacteroidetes, Spirochaetes, Tenericutes (Mollicutes), Acidobacteria, Fibrobacteres, Fusobacteria, Dictyoglomi, Gemmatimonadetes, Lentisphaerae, Verrucomicrobia, Chlamydiae, and Planctomycetes.” *Bergey’s Manual® of Systematic Bacteriology* 1509: 1–19. https://doi.org/10.1007/978-0-387-68572-4_1.

Luo, Jianghan, Heng Liang, Lijun Yan, Jun Ma, Yanling Yang, and Guibai Li. 2013. “Microbial Community Structures in a Closed Raw Water Distribution System Biofilm as Revealed by 454-Pyrosequencing Analysis and the Effect of Microbial Biofilm Communities on Raw Water Quality.” *Bioresource Technology* 148: 189–95.

Ma, Xu, Guiwei Li, Ruya Chen, Ying Yu, Hui Tao, Guangming Zhang, and Baoyou Shi. 2020. "Revealing the Changes of Bacterial Community from Water Source to Consumers Tap: A Full-Scale Investigation in Eastern City of China." *Journal of Environmental Sciences* 87: 331–40. https://doi.org/10.1016/j.jes.2019.07.017.

McBride, Brian W, and Peter C B Turnbull. 1998. "Bacillus, Infection and Immunity." In , edited by Peter J B T - Encyclopedia of Immunology (Second Edition) Delves, 311–15. Oxford: Elsevier. https://doi.org/https://doi.org/10.1006/rwei.1999.0080.

McNeill, Laurie S, and Marc Edwards. 2002. "The Importance of Temperature in Assessing Iron Pipe Corrosion in Water Distribution Systems." *Environmental Monitoring and Assessment* 77 (3): 229–42.

Miller, Keith, Kristina Costa, Donna Cooper, and Mel Evans. 2012. "How to Upgrade and Maintain Our Nation's Wastewater and Drinking-Water Infrastructure ASSOCIATED PRESS/ How to Upgrade and Maintain Our Nation's Wastewater and Drinking-Water Infrastructure," no. October. www.americanprogress.org.

Milwaukee Water Works. 2018. "2018 Milwaukee Water Works Annual Report." Milwaukee, Wisconsin.

Moore, Willard S. 1996. "Large Groundwater Inputs to Coastal Waters Revealed by 226Ra Enrichments." *Nature* 380: 612–14.

Mott, L. 2016. "Hach Chlorine Test Kit."

Mukundan, R., and R. Van Dreason. 2014. "Predicting Trihalomethanes in the New York City Water Supply." *Journal of Environmental Quality* 43 (2): 611–16.

Murray, R. 2004. "The Prokaryotes: An Evolving Electronic Resource for the Mircobiological Community." *Springer-Verlag*.

National Research Council. 2002. *Privatization of Water Services in the United States*. *Privatization of Water Services in the United States*. Washington DC: The National Academies Press. https://doi.org/10.17226/10135.

Nescerecka, Alina, Janis Rubulis, Marius Vital, Talis Juhna, and Frederik Hammes. 2014.

"Biological Instability in a Chlorinated Drinking Water Distribution Network." *PLoS ONE* 9 (5): 1–11. https://doi.org/10.1371/journal.pone.0096354.

Newton, R. J., S. E. Jones, A. Eiler, K. D. McMahon, and S. Bertilsson. 2011. *A Guide to the Natural History of Freshwater Lake Bacteria*. *Microbiology and Molecular Biology Reviews*. Vol. 75. https://doi.org/10.1128/mmbr.00028-10.

Noble, Rachel T., and Jed A. Fuhrman. 1998. "Use of SYBR Green I for Rapid Epifluorescence Counts of Marine Viruses and Bacteria." *Aquatic Microbial Ecology* 14 (2): 113–18. https://doi.org/10.3354/ame014113.

North Shore Water Commission. 2018. "2018 North Shore Water Commission Annual Report." Glendale, Wisconsin.

———. 2020. "Purification." 2020. http://northshorewc.com/splash/treatment/.

NSF International. 2001. "Drinking Water System Components — Health Effects." NSF/ANSI 61 - 2001. 2001. https://law.resource.org/pub/us/cfr/ibr/005/nsf.61.2001.html.

Oren, Aharon. 2014. "The Family Xanthobacteraceae BT - The Prokaryotes: Alphaproteobacteria and Betaproteobacteria." In , edited by Eugene Rosenberg, Edward F DeLong, Stephen Lory, Erko Stackebrandt, and Fabiano Thompson, 709–26. Berlin, Heidelberg: Springer Berlin Heidelberg. https://doi.org/10.1007/978-3-642-30197-1_258.

Parada, A. E., D. M. Needham, and J. A. Fuhrman. 2016. "Every Base Matters: Assessing Small Subunit RRNA Primers for Marine Microbiomes with Mock Communities, Time Series and Global Field Samples." *Environmental Microbiology* 18 (5): 1403–14.

Perrin, Yoann, Didier Bouchon, Vincent Delafont, Laurent Moulin, and Yann Héchard. 2019. "Microbiome of Drinking Water: A Full-Scale Spatio-Temporal Study to Monitor Water Quality in the Paris Distribution System." *Water Research* 149: 375–85. https://doi.org/10.1016/j.watres.2018.11.013.

Pinto, Ameet J., Chuanwu Xi, and Lutgarde Raskin. 2012. "Bacterial Community Structure in the Drinking Water Microbiome Is Governed by Filtration Processes." *Environmental Science and Technology* 46 (16): 8851–59. https://doi.org/10.1021/es302042t.

Pinto, Ameet, Joanna Schroeder, Mary Lunn, William Sloan, and Lutgarde Raskin. 2014. "Spatial-Temporal Survey and Occupancy-Abundance Modeling To." *Mbio* 5 (3): 1–13. https://doi.org/10.1128/mBio.01135-14.Editor.

Potgieter, Sarah, Ameet Pinto, Makhosazana Sigudu, Hein du Preez, Esper Ncube, and Stephanus Venter. 2018. "Long-Term Spatial and Temporal Microbial Community Dynamics in a Large-Scale Drinking Water Distribution System with Multiple Disinfectant Regimes." *Water Research* 139: 406–19. https://doi.org/10.1016/j.watres.2018.03.077.

Prest, Emmanuelle I., Frederik Hammes, Mark C.M. van Loosdrecht, and Johannes S. Vrouwenvelder. 2016. "Biological Stability of Drinking Water: Controlling Factors, Methods, and Challenges." *Frontiers in Microbiology* 7 (FEB): 1–24. https://doi.org/10.3389/fmicb.2016.00045.

Public Service Institute of Wisconsin. 1968. *Opinions and Decisions of the Public Service Commission of Wisconsin*. Madison, WI: Public Service Commission. https://books.google.com/books?id=ASZSAAAAMAAJ&dq=north+shore+water+commission+history+wisconsin&source=gbs_navlinks_s.

RB, Simpson G L, Peter Solymos, M Henry H Stevens, and Helene Wagner. 2013. "Vegan: Community Ecology Package. R Package Version 2.0-10."

Rittman, BE, and VL Snoeyink. 1984. "Achieving Biologically Stable Wate." *Journal / American Water Works Associationof The* 76 (10): 106–14.

Rosenberg, Eugene. 2014. "The Family Chitinophagaceae BT - The Prokaryotes: Other Major Lineages of Bacteria and The Archaea." In , edited by Eugene Rosenberg, Edward F DeLong, Stephen Lory, Erko Stackebrandt, and Fabiano Thompson, 493–95. Berlin, Heidelberg: Springer Berlin Heidelberg. https://doi.org/10.1007/978-3-642-38954-2_137.

Safe Drinking Water Committee, and National Research Council. 1977. *Drinking Water and Health, Volume 1*. Edited by Natinal Academy of Sciences. Vol. 1780. Washington DC: National Academies Press.

Stanford, Benjamin D, Aleksey N Pisarenko, Shane A Snyder, and Gilbert Gordon. 2011. "Perchlorate, Bromate, and Chlorate in Hypochlorite Solutions: Guidelines for Utilities."

Journal AWWA 103 (6): 71–83. https://doi.org/https://doi.org/10.1002/j.1551-8833.2011.tb11474.x.

Tabuchi, Hiroko. 2017. "$300 Billion War Beneath the Street: Fighting to Replace America's Water Pipes." *New York Times*, November 17, 2017. https://www.nytimes.com/2017/11/10/climate/water-pipes-plastic-lead.html.

Tian, Renmao, Daliang Ning, Zhili He, Ping Zhang, Sarah J. Spencer, Shuhong Gao, Weiling Shi, et al. 2020. "Small and Mighty: Adaptation of Superphylum Patescibacteria to Groundwater Environment Drives Their Genome Simplicity." *Microbiome* 8 (1): 1–15. https://doi.org/10.1186/s40168-020-00825-w.

Ushio, Masayuki. 2018. "Use of a Filter Cartridge Combined with Intra-Cartridge Bead Beating Improves Detection of Microbial DNA from Water Samples," 1–19.

Walters, William, Embriette R Hyde, Donna Berg-lyons, Gail Ackermann, Greg Humphrey, Alma Parada, Jack a Gilbert, and Janet K Jansson. 2015. "Transcribed Spacer Marker Gene Primers for Microbial Community Surveys." *MSystems* 1 (1): e0009-15. https://doi.org/10.1128/mSystems.00009-15.Editor.

Wang, Hong, Sheldon Masters, Marc A. Edwards, Joseph O. Falkinham, and Amy Pruden. 2014. "Effect of Disinfectant, Water Age, and Pipe Materials on Bacterial and Eukaryotic Community Structure in Drinking Water Biofilm." *Environmental Science and Technology* 48 (3): 1426–35. https://doi.org/10.1021/es402636u.

Wang, Hong, Sheldon Masters, Yanjuan Hong, Jonathan Stallings, Joseph O. Falkinham, Marc A. Edwards, and Amy Pruden. 2012. "Effect of Disinfectant, Water Age, and Pipe Material on Occurrence and Persistence of Legionella, Mycobacteria, Pseudomonas Aeruginosa, and Two Amoebas." *Environmental Science and Technology* 46 (21): 11566–74. https://doi.org/10.1021/es303212a.

Waples, James T., Jason K. Bordewyk, Kristina M. Knesting, and Kent A. Orlandini. 2015. "Using Naturally Occurring Radionuclides To Determine Drinking Water Age in a Community Water System." *Environmental Science and Technology* 49 (16): 9850–57. https://doi.org/10.1021/acs.est.5b03227.

Waples, James T., and Kent A. Orlandini. 2010. “A Method for the Sequential Measurement of Yttrium-90 and Thorium-234 and Their Application to the Study of Rapid Particle Dynamics in Aquatic Systems.” *Limnology and Oceanography: Methods* 8 (12): 661–77. https://doi.org/10.4319/lom.2010.8.0661.

Weekes, Lan Chi Nguyen, and Donald M. Weekes. 2017. “Legionella Managment for Building Water Systems.” *ASHRAE Journal* 59 (11): 76–79.

Wilmotte, Annick, and Michael Herdman. 2001. “Bergey’s Manual of Systematic Bacteriology. Volume One: The Archaea and the Deeply Branching and Phototrophic Bacteria.”

APPENDICES

Appendix A:Tables

Table A1: Times at which microbial and water chemistry samples were collected.

Sample Name	Date/Time Sampling	Station Name
tap11	9/1/2020 9:34	Treatment Plant
tap12	9/1/2020 9:22	Treatment Plant
tap13	9/1/2020 10:17	5
tap14	9/10/2020 9:02	5
tap15	9/10/2020 9:21	4
tap16	9/15/2020 9:05	3
tap17	9/15/2020 9:25	1
tap18	9/22/2020 9:10	5
tap19	9/22/2020 9:26	4
tap20	10/1/2020 8:10	5
tap21	10/1/2020 8:25	4
tap22	10/1/2020 8:40	3
tap23	10/1/2020 8:55	1
tap24	10/6/2020 9:35	3
tap25	10/6/2020 9:35	1
tap26	10/22/2020 8:35	4
tap27	10/22/2020 8:50	3
tap28	10/22/2020 9:05	1
tap29	10/29/2020 8:35	5
tap30	10/29/2020 8:50	4
tap31	10/29/2020 9:05	3
tap32	11/12/2020 8:35	5
tap33	11/12/2020 8:55	3
tap34	11/12/2020 9:20	1
tap35	11/19/2020 8:35	4
tap36	11/19/2020 8:50	3
tap37	11/19/2020 9:10	1
tap38	12/3/2020 8:30	5
tap39	12/3/2020 9:05	Treatment Plant
tap40	12/3/2020 9:02	Treatment Plant
tap41	12/8/2020 7:52	4
tap42	12/8/20 8:07	3
tap43	12/8/20 8:20	1

Table A2: Times at which radiochemistry samples were collected

sample name	location	date/time sampling
tap11	Treatment Plant	9/1/2020 9:34
tap13	5	9/1/2020 10:17
tap14	5	9/10/2020 9:02
tap15	4	9/10/2020 9:21
tap18	5	9/22/2020 9:10
tap19	4	9/22/2020 9:26
tap20	5	10/1/2020 8:10
tap21	4	10/1/2020 8:25
tap22	3	10/1/2020 8:40
tap23	1	10/1/2020 8:55
tap24	3	10/6/2020 9:35
tap25	1	10/6/2020 9:35
tap26	4	10/22/2020 8:35
tap27	3	10/22/2020 8:50
tap28	1	10/22/2020 9:05
tap30	4	10/29/2020 8:50
tap31	3	10/29/2020 9:05
tap32	5	11/12/2020 8:35
tap33	3	11/12/2020 8:55
tap34	1	11/12/2020 9:20
tap35	4	11/19/2020 8:35
tap36	3	11/19/2020 8:50
tap37	1	11/19/2020 9:10

Table A3: Measured ^{90}Y activities

Sample Name	Station Number	Time Sampled	^{90}Y Activity (dpm L^{-1})
tap11	Treatment plant	9/1/20 9:12	-0.01 ± -0.02
tap13	5	9/1/20 10:17	0.22 ± 0.02
tap14	5	9/10/20 9:02	0.25 ± 0.04
tap15	4	9/10/20 9:21	0.11 ± 0.04
tap18	5	9/22/20 9:10	0.27 ± 0.03

tap19	4	9/22/20 9:26	0.20 ± 0.02
tap20	5	10/1/20 8:10	0.27 ± 0.02
tap21	4	10/1/20 8:25	0.14 ± 0.02
tap22	3	10/1/20 8:40	0.22 ± 0.08
tap23	1	10/1/20 8:55	0.32 ± 0.03
tap24	3	10/6/20 9:10	0.13 ± 0.05
tap25	1	10/6/20 9:25	0.86 ± 0.06
tap26	4	10/22/20 8:35	0.19 ± 0.02
tap27	3	10/22/20 8:50	0.29 ± 0.03
tap28	1	10/22/20 9:05	0.84 ± 0.09
tap30	4	10/29/20 8:50	0.15 ± 0.02
tap31	3	10/29/20 9:10	0.19 ± 0.1
tap32	5	11/12/20 8:35	0.31 ± 0.04
tap33	3	11/12/20 8:55	0.35 ± 0.03
tap34	1	11/12/20 9:20	3.1 ± 0.29
tap35	4	11/19/20 8:35	0.16 ± 0.30
tap36	3	11/19/20 8:50	0.18 ± 0.04
tap37	1	11/19/20 9:15	1.48 ± 0.42

Appendix B: Figures

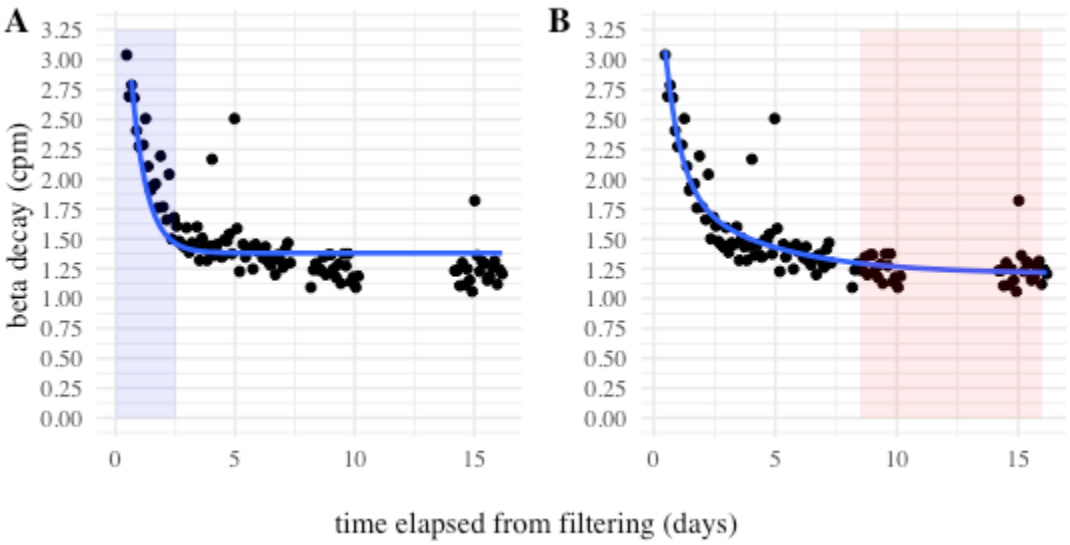

Figure A1: Scatter plot showing the beta decay of tap44 across time with an exponential model with a ^{90}Y decay term (A) and with both a ^{90}Y and ^{212}Pb decay term (B).

With a half-life of 10.64 hours, the influence of ^{212}Pb is most apparent during the first 2.5 days of counting (A, blue rectangle). With the additional decay term, the exponential model was better able to predict the beta decay: The standard error of the estimate decreased from 0.23 to 0.18. Towards the end of the counting period, the influence of longer-lived radionuclides, such as ^{234}Th, can be seen (B, red rectangle). For this reason, counts taken after 8.5 days from filtration were removed from the analysis.